Version of Record: https://www.sciencedirect.com/science/article/pii/S0301932222002750
Manuscript_cc306530f8775d33a07a946d38e87eea

A correction procedure for self-induced velocity of a finite-sized particle in two-way coupled Euler-Lagrange simulations

S. Balachandar[a,*], Kai Liu[a,b*]

[a] *University of Florida, Gainesville, FL 32611, USA*

[b] *State Key Laboratory of Clean Energy Utilization, Zhejiang University, Hangzhou 310027, China*

October 24, 2022

Abstract

The importance of incorporating a correction to undo the self-induced perturbation velocity of a particle, when its size becomes comparable to the Eulerian grid, in a two-way coupled Euler-Lagrange (EL) simulation is now well appreciated. The present work improves upon the prior correction procedures in a few important ways. First, the past correction procedures have been scalar-based with the assumption that the quasi-steady force is the source of self-induced velocity perturbation. Here we generalize to a vector correction procedure and thereby the directions of feedback force and relative velocity can be different. This allows the correction procedure to be used even in the presence of added-mass, history, and lift forces. Second, the effect of a nearby wall has been systematically included in the correction procedure. The correction procedure depends on fundamental Oseen solutions of streamwise and transverse regularized feedback forces. We present a Fourier transform-based analytical approach to obtaining these regularized Oseen solutions. We also present a step-by-step numerical procedure for obtaining the Oseen solutions in any EL code. With the analytical or numerical Oseen functions, the correction procedure can be easily implemented in any EL code. Iterations are required in solving the implicit correction equations and it is demonstrated that the correction procedure converges rapidly within three or four iterations. A simple empirical approach is also presented to account for unsteady effects in the correction procedure.

1 Introduction

In traditional Euler-Lagrange (EL) simulations, the particle size is typically much smaller than the grid size and in this limit the back effect of an individual particle on the flow is generally small. This allows for the force on the particle to be computed in terms of the local fluid velocity without having to correct for the negligible self-induced perturbation caused by the back coupled force. In other words, the effect of the feedback force of an individual particle can be taken to be negligible and the local fluid velocity can be taken to be undisturbed by the particle itself. For a larger particle of size of the order of the grid, the feedback force becomes comparable in magnitude to other forces and alters the local fluid flow. This flow alteration is known as the *self-induced perturbation* of the particle. It is now well recognized that the self-induced perturbation velocity must be corrected in the calculation of the hydrodynamic force on the particle, since the commonly used hydrodynamic force expressions are based on the undisturbed fluid velocity or the far-field velocity of the particle [3; 4; 12].

The widespread recognition of the importance of implementing a correction procedure in EL simulations becomes clear with the rapidly increasing number of correction procedures that have been advanced to recover the undisturbed fluid velocity at the particle, from which the correct hydrodynamic force can be calculated. One of the earliest attempts to accurately account for the self-induced perturbation flow of the particles as steady Stokeslets was by Pan & Banerjee [33]. In the force coupling method advanced by Maxey & co-workers [11; 27; 29] the back coupling of each particle on the surrounding fluid is expressed as a multipole expansion of a regularized steady Stokes solution, where the

*Corresponding Authors: bala1s@ufl.edu, kailiu7777@gmail.com

delta function force has been smoothened to a Gaussian. Gualtieri & co-workers [8; 9; 20] developed the exact-regularized point particle approach where the self-induced correction was obtained as a solution to the unsteady Stokes equation with and without the effect of a nearby wall taken into account. Ireland & Desjardin [23] also used the steady Stokes solution of a Gaussian feedback force to correct for the self-induced perturbation. The low Reynolds number limitation of the above Stokes flow-based self-induced correction procedures can be removed by including the effect of nonlinearity, which was considered by Balachandar & co-workers [5; 26] using analytical solution to the Oseen equation. The Stokes and the Oseen solutions have also been extended to non-Gaussian and nonlinear regularization schemes [15; 34].

There have also been other approaches to correction of self-induced perturbation. Horwitz & Mani [21; 22] developed a correction procedure based on an appropriate weighting of the Laplacian of the computed velocity at the particle. Fukada and co-workers [17] developed feedback force distribution functions that when applied were shown to recover results similar to those of fully-resolved simulations and this approach which initially was developed for a stationary particle was generalized to more complex flows [16]. Esmaily & Horwitz [14] considered the self-induced disturbance velocity to be equivalent to a computational cell where the particle is located being dragged by the feedback force, which was then extended to account for the effect of a nearby wall [32]. More recently, [31] advanced an approach where a globally undisturbed flow can be obtained by numerically solving auxiliary nonlinear equations. This becomes a viable approach in the low volume fraction limit where self-induced perturbations of the different particles do not interact. This approach enjoys the advantage that it is fully nonlinear and is also independent of interpolation functions, and is valid for all forces and wall effects. Clearly there is some connection between the two approaches to self-induced perturbation correction, but the relation between the continuous filter-based approach [5; 15; 23; 34] and the discrete grid or cell-based approach [14; 21; 22; 31; 32] needs further investigation, which shall be considered further in Section 8.

Motivated by the above surge of research, multiphase flow community now requires a comprehensive self-induced perturbation correction procedure with the following desired properties: (i) The correction must be applicable not only for small values of particle Reynolds number, but also for moderate values. In other words, the correction must extend beyond the Stokes flow; (ii) The correction must remain applicable for all kinds of hydrodynamic feedback force (e.g., quasi-steady, added-mass, viscous history and lift forces). As a result, the velocity correction may not be aligned with the feedback force; (iii) The correction must be applicable even in the case of finite volume fraction, where there is interaction with neighboring particles. I.e., the correction must undo only the self-perturbation effect of a particle, while retaining the perturbation effects of neighbors. (iv) The correction procedure must include the effect of nearby boundaries; (v) The correction must accurately handle both quasi-steady and unsteady conditions of rapidly varying feedback force (this requirement is somewhat more general than the requirement that the correction should be applicable for a wide range of particle Stokes number); (vi) When numerically resolved in an appropriate manner, the correction procedure must be independent of numerical details, such as grid size, grid aspect ratio, structured versus unstructured grid, and order of spatial discretization; (vii) The correction must be easily generalizable to any feedback projection (also know as regularization). In other words, the correction procedure must be applicable for Gaussian spreading, particle-in-cell approach [13], discrete delta function spreading[1; 35], or Wendland function smoothening [15]; (viii) The correction procedure must offer the right balance between accuracy and computational efficiency; and (ix) the procedure must be easily implementable in existing EL codes. A universal approach that embodies all these desired properties can be encapsulated into functions and subroutines that can be widely used.

The main purpose of this paper is to work towards the above goal by presenting an efficient correction methodology that can be implemented in existing EL simulation frameworks to obtain the undisturbed flow velocity or recover the correct hydrodynamic force in terms of the fluid properties computed at the particle. We will build upon the correction procedure presented in [5] and seek four generalizations that improve upon the existing procedure: (i) The past scalar-corrections assumed the feedback force on the fluid to be in the direction of relative velocity. Here we will pursue a vector-correction and thereby the directions of feedback force and relative velocity can be different. Directional alignment is appropriate only in the case of quasi-study force, whereas in the presence of added-mass, history, and lift forces, the feedback force on the fluid will not align with the relative velocity vector. (ii) We will include the effect of a nearby wall on the correction process. The presence of a wall is expected to change the self-induced perturbation flow of a particle and therefore the correction procedure must properly account for the modified perturbation.

The correction procedure will be expressed in terms of the fundamental solution of the flow due to a local regu-

larized point forcing in an unbounded uniform cross-flow. Based on the finite Re simulation results presented in [5], the fundamental solution can be well approximated with the Oseen solution to reasonable accuracy. It will be shown that the regularized Oseen solution (referred to as the regularized Oseenlet) reduces to five planar correction functions, which are analytically obtained with the Reynolds number as the only parameter.

With this information, the other two generalizations of the present work can be described. (iii) The influence of numerical methodology employed in an EL simulation on the correction procedure will be assessed in the following way. The regularized Oseen functions will also be computed numerically for both the higher-order spectral method and for the second-order central-difference scheme. By comparing these numerically-generated regularized Oseenlets against those obtained analytically, it will be shown that their difference becomes negligible with adequate spatial resolution. This will establish under what level of numerical resolution the correction is independent of the numerical details. (iv) In addition to Gaussian spreading function, we will also consider hyper-Gaussian spreading functions, which approximate the PIC approach. It will be shown that the resulting regularized Oseenlets are qualitatively very similar for the different spreading functions considered. Furthermore, Evrard *et al.* [15] showed that the correction procedure developed for Gaussian can be easily replicated for other spreading functions. Thus, the user is offered the following two options. Option-1 will be to use the analytic regularized Oseen functions within the overall correction procedure to be outlined here. Option-2 will be for the user to develop the five regularized Oseen functions numerically with their own code following the simple steps to be outlined below and then use these functions within the overall correction procedure. This latter approach has the advantage of taking into account the specific numerical discretization and feedback force implementation that are unique to different codes.

Incorporating the above four modifications are useful steps in the development of a general correction procedure. The reasons are as follows: (i) the misalignment of relative velocity and force vectors is common in the presence of forces other than the quasi-steady contribution, (ii) solid boundaries are typically present in many particle-laden flow applications, and (iii) particle-laden EL simulations use a wide variety of spatial discretization schemes and regularization implementations. For the correction procedure to be computationally simple and efficient, we will employ judicious simplifications that are based on Oseens approximation. The accuracy of the approximation can be evaluated by comparing the results of the correction procedure against corresponding numerical simulations. By following the approach of [5], the proposed method will be appropriate for a wide range of particle Reynolds numbers, adaptable for unsteady conditions, analytically-based, and thus independent of numerical methodology.

Although it is well recognized that self-induced perturbation correction is required when particle size becomes comparable to the grid resolution, the ratio $d_p/\Delta x$ is not always the key controlling factor. In the case of feedback using a spreading function, the feedback force of a particle is projected onto the surrounding fluid through a Gaussian, discrete delta, or Wendland spreading function. If the spreading function is well resolved by the grid, then the correction procedure becomes independent of grid resolution (i.e., independent of $d_p/\Delta x$) and depends on only the width of the spreading function compared to particle diameter (i.e., on d_p/σ). If the spreading function is not adequately resolved by the grid, then the correction procedure will depend on both d_p/σ and $d_p/\Delta x$. In the case of PIC-like approach, feedback is intimately depended on the grid resolution and therefore correction procedure will depend on the ratio $d_p/\Delta x$. The option-1 of analytic Oseen correction function can be pursued in the case of feedback with spreading function with adequate resolution of the spreading function. Both when grid resolution is not adequate and with the use of PIC-like approach one must pursue option-2 and numerically obtain the Oseen correction functions. However, the overall correction procedure remains the same, independent of whether analytic or numerical correction is employed.

The rest of the paper will follow the following plan: first we will rework the steady correction procedure given in [5] to a form that is suitable for present discussion (Section 2). We will then extend this scalar-correction procedure to a general vector form, where the force and the relative velocity vectors are not aligned (Section 3). In Section 4, we will present the five analytic regularized Oseen functions and also present a simple procedure for generating them numerically in any EL code. We will then incorporate the effect of a nearby wall into the vector-correction model using the five regularized Oseen functions. As the final step, we will extend the above correction model to unsteady conditions by adopting the approach of [5] in the vector context (Section 5). The effects of different numerical methodology used in an EL simulation on the correction are discussed in Section 6. The effects of different feedback spreading techniques on the regularized Oseen functions are discussed in Section 7. Two simple simulation tests of varying force dirction with and without a wall are performed to validate the accuracy of the self-induced velocity

correction model in Section 8. Final conclusions are drawn in Section 9.

2 Scalar Formulation of Quasi-Steady Correction

The focus of this subsection is to summarize the scalar-correction procedure of [5] and present their Oseen solution in a manner that is suitable for extension to vectorial form and easy implementation in a two-way coupled EL simulation. Consider a particle in an EL simulation, whose location is chosen to be the origin of the coordinate system. This particle will be called the "reference particle" and the focus here is to obtain the correct undisturbed fluid velocity of this particle so that the hydrodynamic force on it can be accurately calculated. Let the fluid velocity computed in the EL simulation be denoted as $\mathbf{u}_c(\mathbf{x}, t)$. This flow field has been computed with the reference particle and its back effect on the fluid included in the simulation. Instead, consider the related EL flow field $\mathbf{U}(\mathbf{x}, t)$, where the presence of the reference particle and its back effect have been ignored. But the flow $\mathbf{U}(\mathbf{x}, t)$ includes the effect of all other particles. This flow field is termed the undisturbed velocity of the reference particle and therefore the force on the reference particle must be evaluated based on $\mathbf{U}(\mathbf{x}, t)$ instead of $\mathbf{u}_c(\mathbf{x}, t)$. Since only $\mathbf{u}_c(\mathbf{x}, t)$ is computed in an actual EL simulation, the first step is to recover the undisturbed velocity $\mathbf{U}(\mathbf{x}, t)$. In fact, the entire velocity field is not needed. Only the average of $\mathbf{U}(\mathbf{x}, t)$ over the surface of the reference particle is needed in the calculation of the hydrodynamic force.

2.1 Volume Effect

There are two sources that contribute to the difference between $\mathbf{U}(\mathbf{x}, t)$ and $\mathbf{u}_c(\mathbf{x}, t)$: the volume effect and the feedback force effect of the reference particle. We first consider the volume effect, where we note that in many EL simulations of dilute multiphase flows, the dispersed phase's volume effect is ignored by taking the fluid volume fraction $\phi_c(\mathbf{x}, t)$ to be unity everywhere in the fluid phase governing equations. In which case, the volume effect of the reference particle does not contribute to the difference between $\mathbf{U}(\mathbf{x}, t)$ and $\mathbf{u}_c(\mathbf{x}, t)$. If the EL governing equations accounted for the spatio-temporal variation of $\phi_c(\mathbf{x}, t)$, then the volume effect of the reference particle must be corrected. The velocity field after correcting for the volume effect can be easily obtained as $\phi_{1c}(\mathbf{x})\, \mathbf{u}_c(\mathbf{x}, t)$, and thus multiplication by $\phi_{1c}(\mathbf{x})$ corrects for the volume effect, where

$$\phi_{1c}(\mathbf{x}) = 1 - \int I_p(\mathbf{x}')\, G(\mathbf{x} - \mathbf{x}')\, d\mathbf{x}' \tag{1}$$

is the fluid volume fraction field with only the reference particle located at the origin. Here the subscript $1c$ represents the volume fraction of the continuous phase in the presence of only one particle located at the origin. In the above, I_p is the indicator function that is unity insider the region occupied by the reference particle ($|\mathbf{x}| < d_p/2$) and zero everywhere outside. Following [5; 10] we take the filter function used in regularization to be isotropic Gaussian function

$$G(\boldsymbol{\xi}) = \frac{1}{(2\pi)^{3/2}\sigma^3} \exp\left(-\frac{|\boldsymbol{\xi}|^2}{2\sigma^2}\right), \tag{2}$$

where σ is the parameter that controls the width of the Gaussian. With this definition, (1) can be integrated and the correction function of the volume effect can be expressed as

$$\phi_{1c}(\mathbf{x}) = 1 - \frac{\mathrm{erf}(A) - \mathrm{erf}(B)}{2} - \frac{\exp(-A^2) - \exp(-B^2)}{\sqrt{\pi}(A + B)}, \tag{3}$$

where $A = (2|\mathbf{x}| + d_p)/(2\sqrt{2}\sigma)$, $B = (2|\mathbf{x}| - d_p)/(2\sqrt{2}\sigma)$, and d_p is the diameter of the particle. The volume correction function ϕ_{1c} has the lowest value at the center of the reference particle and increases rapidly to 1 farther away. Plots of $\phi_{1c}(\mathbf{x})$ versus $|\mathbf{x}|/d_p$ for $\sigma/d_p = 0.3$, 0.5, 1, and 2 are shown in Figure 1. The inset in the figure shows the value of $\phi_{1p} = 1 - \phi_{1c}$ at the center of the particle (where $[\cdot]_@$ denotes $|\mathbf{x}| = 0$) as a function of σ/d_p. A value of ϕ_{1c} much lower than unity corresponds to substantial volume fraction effect. Therefore, it is clear that volume effect is substantial $\phi_{1p} \gtrapprox 3\%$ only for σ/d_p smaller than unity. At larger values of σ/d_p, the volume of the particle is distributed over a much larger region so that $\phi_{1c} \approx 1$ over the entire volume.

The volume effect can be understood as the result of mass balance given by $\nabla \cdot (\phi_{1c}\mathbf{u}_c) = 0$. In the context of a steady uniform undisturbed ambient flow (i.e., $\mathbf{U}(\mathbf{x}, t) = \mathbf{U}_0$), in the presence of the reference particle at the origin, with no other force on the fluid, the EL velocity field is given by $\mathbf{u}_c(\mathbf{x}, t) = \mathbf{U}_0/\phi_{1c}(\mathbf{x})$. In other words, the EL velocity increases near the origin due to the volume effect of the reference particle - the uniform flow has to squeeze through the volume available for the fluid flow exterior of the particle. Thus, by multiplying the velocity field $\mathbf{u}_c$ computed in an EL simulation with ϕ_{1c} we undo the volume effect of the reference particle.

Here we remark that in EL simulations, the integral in the volume fraction definition in (1) is often approximated as [23]

$$\phi_{1c}(\mathbf{x}) \approx 1 - V_p \int \delta(\mathbf{x}')\, G(\mathbf{x} - \mathbf{x}')\, d\mathbf{x}' = 1 - V_p G(|\mathbf{x}|)\,, \tag{4}$$

where $V_p = \pi d_p^3/6$ is the particle volume. This approximation is also plotted in Figure 1. It is clear that the approximation is very good with error

$$\left.\frac{\left|[\phi_{1p}]_{@}^{\text{Approximation}} - [\phi_{1p}]_{@}^{\text{Analytical}}\right|}{[\phi_{1p}]_{@}^{\text{Approximation}}}\right|_{\sigma/d_p=1} < 7.73\%$$

provided $\sigma/d_p > 1$. For larger particles, the difference is substantial and one should not use the approximation. For $\sigma/d_p \lessapprox 0.3$ the approximation given in (4) becomes negative, while the exact result given in (3) remains well behaved for all values of filter width. Even for larger values of σ/d_p, the approximation (4), when applied for all the particles within a system to calculate the fluid volume fraction field, can lead to unrealistically small or even negative values in regions where particles cluster. Furthermore, as will be discussed later, even in a dilute distribution of particles, as a particle gets closer to a boundary, edge, or corner of the computational domain, superposition of the particle and its one, three, or seven images is required, which again can lead to incorrect evaluation of ϕ_{1c}. Therefore, in an EL simulation, the actual volume fraction field $\phi_c(\mathbf{x}, t)$ of a distribution of particles should be obtained from a superposition of (3), which is recommended over a similar superposition of the approximation given in (4).

The difference between the volume correction $\phi_{1c}(\mathbf{x})$ and the EL volume fraction field $\phi_c(\mathbf{x}, t)$ must be stressed. The former is the volume fraction field of only the reference particle, whereas $\phi_c(\mathbf{x}, t)$ computed in an EL simulation takes into account the presence of all the particles within the domain. The volume correction must only correct for the presence of the reference particle and should not be affected by the presence of all other particles. This is the reason why the correction uses the volume fraction field ϕ_{1c} of only the reference particle. Fortunately, unlike ϕ_c, the function ϕ_{1c} needed in the correction is independent of how particles are distributed in an EL simulation.

2.2 Feedback Force Effect

We now focus on the contribution to the difference between $\mathbf{U}(\mathbf{x}, t)$ and $\mathbf{u}_c(\mathbf{x}, t)$ due to the feedback force $-\mathbf{F}'(t)G(\mathbf{x})$ applied to the fluid, where $\mathbf{F}'(t)$ is the hydrodynamic force on the reference particle (here prime indicates that this feedback force does not include the pressure gradient or the stress-divergence force, which is the undisturbed flow force - only the force due to flow disturbance is fed back to the fluid). Let the self-induced perturbation flow due to this Gaussian feedback force be $\mathbf{u}'_{1c}(\mathbf{x}, t)$, whose analytic solution in the Oseen limit was presented in [5] (the subscript $1c$ emphasizes the fact that this solution is obtained with only the reference particle, without the presence of all other particles). Together, we obtain the result

$$\underbrace{\mathbf{U}(\mathbf{x}, t)}_{\substack{\text{True undisturbed}\\ \text{velocity}}} = \underbrace{\phi_{1c}\mathbf{u}_c(\mathbf{x}, t)}_{\substack{\text{EL velocity}\\ \text{with volume correction}}} - \underbrace{\phi_{1c}\mathbf{u}'_{1c}(\mathbf{x}, t)}_{\substack{\text{Perturbation velocity}\\ \text{due to feedback}}}\,. \tag{5}$$

By taking the second term on the right to the left hand side, the above equation can be interpreted as the computed EL velocity to be the true undisturbed velocity of the reference particle plus its self-induced perturbation, and multiplication by ϕ_{1c} corrects for the volume effect. The above equation can be used to obtain the true undisturbed velocity of a particle in an EL simulation by making it the reference particle and subtracting its self-induced perturbation.

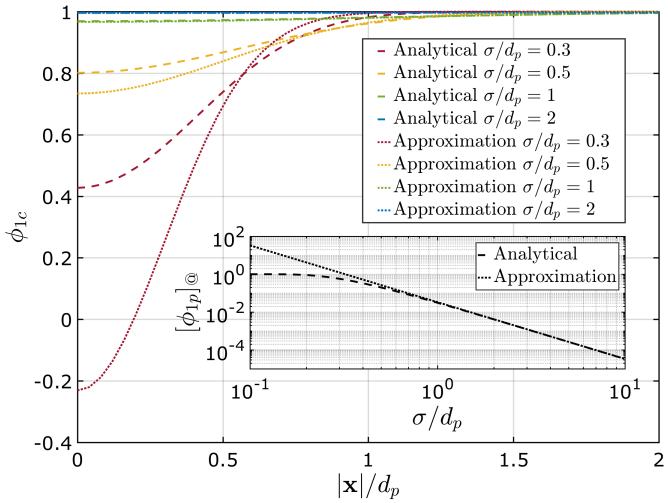

Figure 1: Plot of the fluid volume fraction using the analytical (3) (dashed) and approximation (4) (dotted) equations with respect to the relative distance between the evaluation position and the particle center. The deviation from unity decreases with increasing Gaussian width. It should be noted that too small a Gaussian width incurs unphysical (negative) fluid volume fraction around the particle center for the approximation equation, while the analytical equation avoids this problem. The inset figure shows the particle volume fraction at the particle center with respect to the Gaussian width. The analytical and approximation results nearly overlap for Gaussian width of the order of a particle diameter or larger.

In the quasi-steady limit, the force on the reference particle can be expressed as

$$\mathbf{F}'_{qs} = 3\pi\mu d_p \left(\overline{\mathbf{U}}^s - \mathbf{V}\right)\Phi \approx 3\pi\mu d_p \left(\mathbf{U}_@ + \frac{d_p^2}{24}\left[\nabla^2\mathbf{U}\right]_@ - \mathbf{V}\right)\Phi\,, \tag{6}$$

where $\mathbf{V}$ is the particle velocity and the operation $\overline{(\cdot)}^s$ denotes an average over the surface of the reference particle. Note that the quasi-steady drag of the reference particle has been correctly expressed in terms of its undisturbed flow. Defining the fluid velocity to be the average over the surface of the particle is rigorous in the Stokes limit. At finite Reynolds number, the surface average is not rigorous. Furthermore, the surface average can be approximated by Taylor series expansion given by the second equality, where the notation $[\cdot]_@$ denotes the quantity being evaluated at the center of the reference particle. The purpose of the surface average or the Taylor series is to account for the fact that $\mathbf{U}$ varies on the scale of the particle when the particle becomes comparable to the grid size, which is the situation of interest to self-induced correction. In the above, $\Phi = 1 + 0.15\,\mathrm{Re}^{0.687}$ is the finite Reynolds number modification of the Stokes drag, where particle Reynolds number based on relative velocity is given by $\mathrm{Re} = d_p|\overline{\mathbf{U}}^s - \mathbf{V}|/\nu$. In the above, μ and ν are the dynamic and kinematic viscosities of the fluid.

Before we substitute (5) into (6), we present the following result of the Oseen analysis given in [5]

$$\overline{\phi_{1c}\mathbf{u}'_{1c}}^s \approx [\phi_{1c}\mathbf{u}'_{1c}]_@ + \frac{d_p^2}{24}\left[\nabla^2(\phi_{1c}\mathbf{u}'_{1c})\right]_@ = -\frac{\mathbf{F}'_{qs}}{6\pi\,\mu\sigma}\sqrt{\frac{2}{\pi}}\underbrace{\left[\Psi_{x\text{-}os} - \frac{1}{24}\frac{d_p^2}{\sigma^2}\Psi_{x\text{-}Lap}\right]}_{\Psi_{x\text{-}ef}}\,. \tag{7}$$

The two functions that appear on the right hand side only depend on the Reynolds number based on Gaussian filter

width, which is defined as $\mathrm{Re}_\sigma = \sigma|\overline{\mathbf{U}}^s - \mathbf{V}|/\nu$. Their dependence have been analytically obtained as [5]

$$\begin{aligned}\Psi_{x\text{-}os}(\mathrm{Re}_\sigma) &= \frac{3}{\sqrt{2\pi}\,\mathrm{Re}_\sigma^3}\left[\pi - \sqrt{2\pi}\,\mathrm{Re}_\sigma + \frac{\pi}{2}\,\mathrm{Re}_\sigma^2 - \pi\exp\left(\frac{\mathrm{Re}_\sigma^2}{2}\right)\mathrm{erfc}\left(\frac{\mathrm{Re}_\sigma}{\sqrt{2}}\right)\right] \\ \Psi_{x\text{-}Lap}(\mathrm{Re}_\sigma) &= \frac{3}{\sqrt{2\pi}\,\mathrm{Re}_\sigma^3}\left[4\pi - 4\sqrt{2\pi}\,\mathrm{Re}_\sigma + \pi\,\mathrm{Re}_\sigma^2 + \pi\,(\mathrm{Re}_\sigma^2 - 4)\exp\left(\frac{\mathrm{Re}_\sigma^2}{2}\right)\mathrm{erfc}\left(\frac{\mathrm{Re}_\sigma}{\sqrt{2}}\right)\right].\end{aligned} \tag{8}$$

Substituting (7) and (5) into (6) we obtain the following important result for the *corrected quasi-steady drag*

$$\mathbf{F}'_{qs} = \underbrace{\left(1 - \frac{d_p}{\sigma}\frac{\Phi\Psi_{x\text{-}ef}}{\sqrt{2\pi}}\right)^{-1}}_{\text{feedback correction}} 3\pi\mu d_p\left(\overline{\phi_{1c}\mathbf{u}_c}^s - \mathbf{V}\right)\,\Phi\,, \tag{9}$$

where the surface average of the EL velocity can be approximated as $\overline{\phi_{1c}\mathbf{u}_c}^s = [\phi_{1c}\mathbf{u}_c]_{@} + (d_p^2/24)\left[\nabla^2(\phi_{1c}\mathbf{u}_c)\right]_{@}$. Note that multiplication of EL velocity by ϕ_{1c} corrects for the volume effect, while the multiplicative term on the right hand side corrects for the feedback effect. The above can be substituted back to obtain the following expression for the *true relative velocity*

$$\left(\overline{\mathbf{U}}^s - \mathbf{V}\right) = \underbrace{\left(1 - \frac{d_p}{\sigma}\frac{\Phi\Psi_{x\text{-}ef}}{\sqrt{2\pi}}\right)^{-1}}_{\text{feedback correction}}\left(\overline{\phi_{1c}\mathbf{u}_c}^s - \mathbf{V}\right)\,. \tag{10}$$

The feedback correction for relative velocity is identically the same as that for quasi-steady force. The correction increases the estimate of true relative velocity to be larger than that obtained from the EL velocity field. Accordingly, the correction also increases the estimate of true quasi-steady force. In both cases, the correction increases as the size of the particle approaches the filter size. The above functional form of feedback force correction was obtained by Esmaily & Horwitz [14] in the quasi-steady regime by considering the fluid within the grid cell to behave as a particle in response to the feedback force acting on it.

The above corrections are easy to implement in any EL simulation as they involve only algebraic operations. Since both Φ and $\Psi_{x\text{-}ef}$ depend on $\overline{\mathbf{U}}^s - \mathbf{V}$, equation (10) is an implicit equation, which may require an iterative solution. It must be noted that for simplicity the above correction procedure relies only upon the Oseen solution. Balachandar et al. [5] observed the nonlinear effects beyond the Oseen solution to be small for practical values of the feedback force and thus the above simple approach is perhaps sufficient for many applications.

3 Vectorial Formulation of Quasi-Steady Correction

The analysis of the above section assumed the feedback force $\mathbf{F}'$ to be only the quasi-steady force. As a result, the feedback force, the relative velocity between the fluid and the particle computed in the EL simulation $\left(\overline{\phi_{1c}\mathbf{u}_c}^s - \mathbf{V}\right)$, the true relative velocity $\overline{\mathbf{U}}^s - \mathbf{V}$, and the self-induced perturbation velocity $\overline{\phi_{1c}\mathbf{u}'_{1c}}^s$ are taken to be oriented along the same direction. Thus, a scalar correction factor was sufficient to relate them in equations (9) and (10). In this section, we will generalize the results by considering the feedback force on the fluid to include not only the quasi-steady contribution but also contributions from added-mass, history and lift forces. We will represent this as

$$\mathbf{F}' = \mathbf{F}'_{qs} + \mathbf{F}'_{ot}\,, \tag{11}$$

where $\mathbf{F}'_{ot}$ indicates the sum of all non-quasi-steady feedback forces. Note that, by definition $\mathbf{F}'_{qs}$ is aligned along the direction of true relative velocity $\overline{\mathbf{U}}^s - \mathbf{V}$, while the direction of $\mathbf{F}'_{ot}$ is not similarly restricted.

We address this general scenario by considering the following Oseen problem, where the undisturbed ambient flow in the frame attached to the particle is of uniform magnitude and directed along the x direction (i.e., $U_r\mathbf{e}_x = \overline{\mathbf{U}}^s - \mathbf{V}$), while the feedback force $\mathbf{F}'$ is not aligned with the flow but oriented in the $x-y$ plane:

$$\begin{aligned}\nabla\cdot(\phi_{1c}\mathbf{u}'_{1c}) &= 0 \\ \rho\,U_r\mathbf{e}_x\cdot\nabla(\phi_{1c}\mathbf{u}'_{1c}) &= -\nabla(\phi_{1c}p'_{1c}) + \mu\nabla^2(\phi_{1c}\mathbf{u}'_{1c}) - (F'_x\mathbf{e}_x + F'_y\mathbf{e}_y)\,G(\mathbf{x})\,.\end{aligned} \tag{12}$$

The x and y components of the feedback force F'_x and F'_y are applied with the regularization function G centered about the origin (here we use the Gaussian filter of width σ). In the above, ρ and μ are the constant density and dynamic viscosity of the fluid. Following the approach outlined in [5], the non-dimensional solution to the above Oseen equation depends only on the Gaussian Reynolds number, which is defined as $\mathrm{Re}_\sigma = \rho U_r \sigma/\mu$. The solution to the above linear equation has two parts, and they scale linearly with F'_x and F'_y, respectively.

The above equation can be solved in Fourier space and transformed back to the physical space. The steps have been presented in [5; 36] and will not be repeated. The streamwise and cross-stream self-induced perturbation velocities averaged over the particle surface can be expressed as

$$\begin{aligned}
\overline{\phi_{1c} u'_{1c}}^s &\approx [\phi_{1c} u'_{1c}]_@ + \frac{d_p^2}{24}\left[\nabla^2(\phi_{1c} u'_{1c})\right]_@ &&= -\frac{F'_x}{6\pi\,\mu\sigma}\sqrt{\frac{2}{\pi}}\underbrace{\left[\Psi_{x\text{-}os} - \frac{1}{24}\frac{d_p^2}{\sigma^2}\Psi_{x\text{-}Lap}\right]}_{\Psi_{x\text{-}ef}} \\
\overline{\phi_{1c} v'_{1c}}^s &\approx [\phi_{1c} v'_{1c}]_@ + \frac{d_p^2}{24}\left[\nabla^2(\phi_{1c} v'_{1c})\right]_@ &&= -\frac{F'_y}{6\pi\,\mu\sigma}\sqrt{\frac{2}{\pi}}\underbrace{\left[\Psi_{y\text{-}os} - \frac{1}{24}\frac{d_p^2}{\sigma^2}\Psi_{y\text{-}Lap}\right]}_{\Psi_{y\text{-}ef}},
\end{aligned} \tag{13}$$

where $\Psi_{x\text{-}os}$ and $\Psi_{x\text{-}Lap}$ have already been given in (8). The corresponding functions for the y-component are expressed as

$$\begin{aligned}
\Psi_{y\text{-}os}(\mathrm{Re}_\sigma) &= \frac{3}{2\sqrt{2\pi}\,\mathrm{Re}_\sigma^3}\left[-\pi + \sqrt{2\pi}\,\mathrm{Re}_\sigma + \frac{\pi}{2}\,\mathrm{Re}_\sigma^2 - \pi(\mathrm{Re}_\sigma^2 - 1)\exp\left(\frac{\mathrm{Re}_\sigma^2}{2}\right)\mathrm{erfc}\left(\frac{\mathrm{Re}_\sigma}{\sqrt{2}}\right)\right] \\
\Psi_{y\text{-}Lap}(\mathrm{Re}_\sigma) &= \frac{3}{2\sqrt{2\pi}\,\mathrm{Re}_\sigma^3}\left[(\mathrm{Re}_\sigma^2 - 4)(\pi - \sqrt{2\pi}\,\mathrm{Re}_\sigma) + \pi(\mathrm{Re}_\sigma^4 - 3\,\mathrm{Re}_\sigma^2 + 4)\exp\left(\frac{\mathrm{Re}_\sigma^2}{2}\right)\mathrm{erfc}\left(\frac{\mathrm{Re}_\sigma}{\sqrt{2}}\right)\right].
\end{aligned} \tag{14}$$

Figure 2 shows $\Psi_{x\text{-}ef}$ and $\Psi_{y\text{-}ef}$ plotted as functions of Re_σ for varying values of d_p/σ. The limiting curves for $d_p/\sigma = 0$ can be interpreted as $\Psi_{x\text{-}os}$ and $\Psi_{y\text{-}os}$ The values of $\Psi_{x\text{-}ef}$ and $\Psi_{y\text{-}ef}$ are nearly unity for $\mathrm{Re}_\sigma \lessapprox 0.1$, but rapidly decrease with increasing Re_σ. In the limit $\mathrm{Re}_\sigma \to 0$, all the functions approach the limiting value of unity. The large Re_σ asymptotic behavior of the different functions are

$$\mathrm{Re}_\sigma \to \infty: \quad \Psi_{x\text{-}os} = \frac{1}{2}\Psi_{y\text{-}os} = 2\Psi_{x\text{-}Lap} = \Psi_{y\text{-}Lap} = \frac{3}{2\,\mathrm{Re}_\sigma}\sqrt{\frac{\pi}{2}}. \tag{15}$$

From these we obtain the corresponding limiting behaviors $\Psi_{x\text{-}ef} = \Psi_{y\text{-}ef}/2 = (1 - \frac{d_p^2}{48\sigma^2})\sqrt{\frac{\pi}{2}}\frac{3}{2\,\mathrm{Re}_\sigma}$. For $\mathrm{Re}_\sigma \gtrapprox 3$ these approximations can be used to simplify calculation. In the implementation of the correction procedure to be presented below as Algorithms-1 and 2, in order to avoid singularity in the calculation of the correction functions (8) and (14), we suggest using the asymptotic solutions for $\mathrm{Re}_\sigma < 0.001$ and $\mathrm{Re}_\sigma > 10$. These asymptotic solutions were used in Figure 2 demonstrating their accuracy and smoothness.

Considering the separation of the feedback force given in (11), we identify the quasi-steady force to only contribute to F'_x, since it is aligned in the direction of relative velocity, while the other feedback force component contributes to both the x and y components. Thus, (13) can be rewritten in the following vectorial form

$$\overline{\phi_{1c}\mathbf{u}'_{1c}}^s \approx -\frac{1}{6\pi\,\mu\sigma}\sqrt{\frac{2}{\pi}}\mathbf{M}^T\,\mathbf{B}_0\,\mathbf{M}\,\left(\mathbf{F}'_{qs} + \mathbf{F}'_{ot}\right), \tag{16}$$

where the unitary rotation matrix $\mathbf{M}$ and the diagonal scaling matrix $\mathbf{B}_0$ are given as

$$\mathbf{M} = \begin{bmatrix} \leftarrow & \mathbf{a} & \rightarrow \\ \leftarrow & \mathbf{b} & \rightarrow \\ \leftarrow & \mathbf{c} & \rightarrow \end{bmatrix} \quad \text{and} \quad \mathbf{B}_0 = \begin{bmatrix} \Psi_{x\text{-}ef} & 0 & 0 \\ 0 & \Psi_{y\text{-}ef} & 0 \\ 0 & 0 & \Psi_{z\text{-}ef} \end{bmatrix}. \tag{17}$$

In the above, the row vector $\mathbf{a}$ is the unit vector along the true relative velocity, $\mathbf{b}$ is the unit vector that is in the $x-y$ plane but normal to $\mathbf{a}$, and $\mathbf{c} = \mathbf{a} \times \mathbf{b}$ is the unit vector normal to the other two. Thus, the term $\mathbf{M}\,\mathbf{F}'_{ot}$ corresponds to

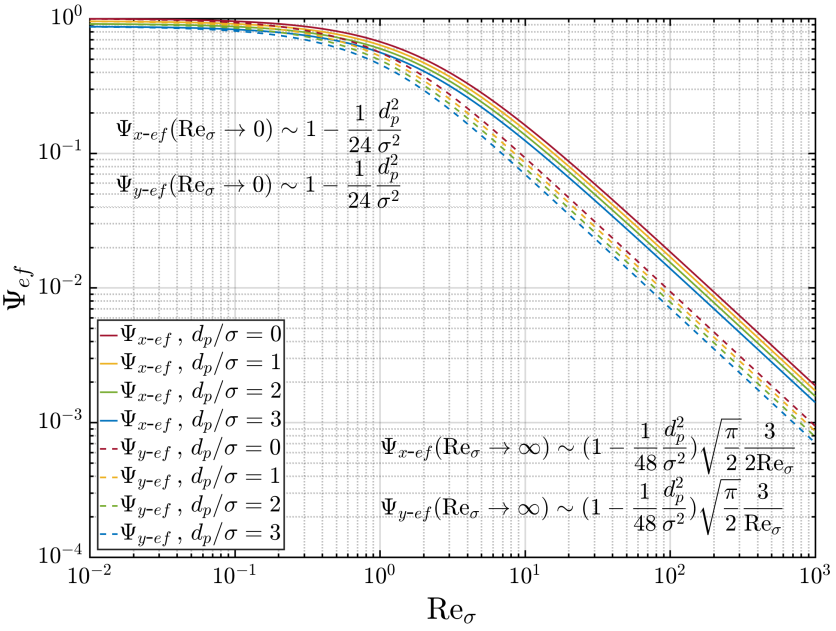

Figure 2: Plot of $\Psi_{x\text{-}ef}$ and $\Psi_{y\text{-}ef}$ as functions Re_σ for varying values of $d_p/\sigma = [0, 1, 2, 3]$. The red lines correspond to the limit $d_p/\sigma = 0$ and are therefore the functions $\Psi_{x\text{-}os}$ (solid) and $\Psi_{y\text{-}os}$ (dashed).

projecting $\mathbf{F}'_{ot}$ along the x and y directions, which are then scaled by the diagonal matrix $\mathbf{B}_0$ and then projected back to the original coordinate system by the transpose $\mathbf{M}^T$. It is straightforward to show that $\Psi_{z\text{-}os} \equiv \Psi_{y\text{-}os}$, $\Psi_{z\text{-}Lap} \equiv \Psi_{y\text{-}Lap}$, and $\Psi_{z\text{-}ef} \equiv \Psi_{y\text{-}ef}$. Although in the current coordinates, $\Psi_{z\text{-}ef}$ is unnecessary since $\mathbf{e}_z \cdot \mathbf{M}\mathbf{F}'_{ot} = 0$, it will be used in the next section of wall boundary condition.

Substituting (16) and (5) into (6) we obtain the following vector form of the *corrected quasi-steady drag*

$$\mathbf{F}'_{qs} = \underbrace{\left(\mathbf{I} - \frac{d_p}{\sigma}\frac{\Phi}{\sqrt{2\pi}}\mathbf{M}^T\,\mathbf{B}_0\,\mathbf{M}\right)^{-1}}_{\text{feedback correction}}\left[3\pi\mu d_p\left(\overline{\phi_{1c}\mathbf{u}_c}^s - \mathbf{V}\right)\Phi + \frac{d_p\Phi}{\sigma\sqrt{2\pi}}\mathbf{M}^T\,\mathbf{B}_0\,\mathbf{M}\,\mathbf{F}'_{ot}\right]. \tag{18}$$

From the above, it is clear that if $\mathbf{F}'_{ot}$ is non-zero, then the corrected quasi-steady drag is not aligned with the relative velocity $\left(\overline{\phi_{1c}\mathbf{u}_c}^s - \mathbf{V}\right)$ of the EL simulation. $\mathbf{F}'_{qs}$ is aligned only with the true relative velocity. Furthermore, the above correction assumes that only the quasi-steady force is affected by self-induced perturbation, In reality, even the added-mass and other forces represented by $\mathbf{F}'_{ot}$ will be modified by self-induced perturbation. Here we make use of the result obtained in [5] that the effect of self-induced perturbation on quasi-steady force is much stronger than those on the other force components. The above can be substituted back to obtain the following expression for the *true relative velocity*

$$\left(\overline{\mathbf{U}}^s - \mathbf{V}\right) = \underbrace{\left(\mathbf{I} - \frac{d_p}{\sigma}\frac{\Phi}{\sqrt{2\pi}}\mathbf{M}^T\,\mathbf{B}_0\,\mathbf{M}\right)^{-1}}_{\text{feedback correction}}\left(\overline{\phi_{1c}\mathbf{u}_c}^s - \mathbf{V} + \frac{1}{6\pi\,\mu\sigma}\sqrt{\frac{2}{\pi}}\mathbf{M}^T\,\mathbf{B}_0\,\mathbf{M}\,\mathbf{F}'_{ot}\right). \tag{19}$$

The feedback correction function is implicit in nature, due to the dependence of Φ on Re and $\Psi_{x\text{-}ef}$ on Re_σ. These two Reynolds numbers are defined in terms of the true relative velocity. Therefore, as shown below, they must be expressed as:

$$\mathrm{Re} = \frac{|\overline{\mathbf{U}}^s - \mathbf{V}|d_p}{\nu} = \left|\left(\mathbf{I} - \frac{d_p}{\sigma}\frac{\Phi}{\sqrt{2\pi}}\mathbf{M}^T\,\mathbf{B}_0\,\mathbf{M}\right)^{-1}\left(\mathrm{Re}_{EL}\,\mathbf{e}_{r,EL} + \frac{d_p}{6\pi\,\mu\sigma\nu}\sqrt{\frac{2}{\pi}}\mathbf{M}^T\,\mathbf{B}_0\,\mathbf{M}\,\mathbf{F}'_{ot}\right)\right|, \tag{20}$$

$$\mathrm{Re}_\sigma = \frac{|\overline{\mathbf{U}}^s - \mathbf{V}|\sigma}{\nu} = \left| \left(\mathbf{I} - \frac{d_p}{\sigma} \frac{\Phi}{\sqrt{2\pi}} \mathbf{M}^T \, \mathbf{B}_0 \, \mathbf{M} \right)^{-1} \left(\mathrm{Re}_{\sigma,EL} \, \mathbf{e}_{r,EL} + \frac{1}{6\pi \, \mu\nu} \sqrt{\frac{2}{\pi}} \mathbf{M}^T \, \mathbf{B}_0 \, \mathbf{M} \, \mathbf{F}'_{ot} \right) \right| , \qquad (21)$$

where $\mathrm{Re}_{EL} = (|\overline{\phi_{1c}\mathbf{u}_c}^s - \mathbf{V}|d_p)/\nu$ and $\mathrm{Re}_{\sigma,EL} = (|\overline{\phi_{1c}\mathbf{u}_c}^s - \mathbf{V}|\sigma)/\nu$ are the Reynolds numbers computed in the EL simulation. Also $\mathbf{e}_{r,EL}$ is the unit vector in the direction of EL relative velocity $(\overline{\phi_{1c}\mathbf{u}_c}^s - \mathbf{V})$. Note that the two Reynolds numbers are related as $\mathrm{Re} = (d_p/\sigma)\,\mathrm{Re}_\sigma$ and $\mathrm{Re}_{EL} = (d_p/\sigma)\,\mathrm{Re}_{\sigma,EL}$. The above are implicit expressions for Re and Re_σ, which can be solved for any value of Re_{EL} computed in an EL simulation, with the additional information of d_p/σ and $\mathbf{F}'_{ot}$.

In summary, in the quasi-steady regime, the problem of self-induced velocity correction for a particle can be stated as follows: Given the particle velocity $\mathbf{V}$ and the local surface-averaged volume-corrected fluid velocity $\overline{\phi_{1c}\mathbf{u}_c}^s$, along with other information such as d_p and ν, we want to calculate the correct quasi-steady force on the particle based on its true relative velocity. This evaluation can be achieved by pursuing the following steps.

Algorithm-1: Quasi-steady Self-induced Correction (away from boundaries)

1. As pre-processing step compute and store the functions $\Psi_{x\text{-}ef}$, $\Psi_{y\text{-}ef}$, and $\Psi_{z\text{-}ef}$, which appear as the diagonal elements of the operator $\mathbf{B}_0$.
2. Compute the time-dependent quantity $\mathbf{F}'_{ot}$.
3. Compute the EL particle Reynolds number as $\mathrm{Re}_{EL} = |\overline{\phi_{1c}\mathbf{u}_c}^s - \mathbf{V}|d_p/\nu$ and the unitary vector $\mathbf{e}_{r,EL} = (\overline{\phi_{1c}\mathbf{u}_c}^s - \mathbf{V})/|\overline{\phi_{1c}\mathbf{u}_c}^s - \mathbf{V}|$.
4. Start the iteration with the initial assumption that the true relative velocity is the same as EL relative velocity. I.e., set $\mathrm{Re} = \mathrm{Re}_{EL}$, $\mathrm{Re}_\sigma = (\sigma/d_p)\,\mathrm{Re}_{EL}$, and $\mathbf{e}_r = \mathbf{e}_{r,EL}$.
5. Compute the values of $\mathbf{M}$, $\mathbf{M}^T$, $\mathbf{B}_0$, and Φ.
6. Apply the correction given in (19) to calculate an improved estimate of the true relative velocity.
7. Use the updated true relative velocity to obtain improved estimates of Re, Re_σ, and $\mathbf{e}_r$.
8. Go back to step 5 and iterate till convergence.
9. Once converged, use (18) to obtain the true quasi-steady force.

In the vectorial form, the feedback corrections along the different coordinate directions depend on the orientation of the relative velocity. Nevertheless, along the direction of true relative velocity, the correction function becomes $\left(1 - d_p\Phi\Psi_{x\text{-}ef}/(\sigma\sqrt{2\pi})\right)^{-1}$ and its BBO limit becomes $\left(1 - d_p\Phi\Psi_{x\text{-}os}/(\sigma\sqrt{2\pi})\right)^{-1}$. These two functions are plotted against Re_σ for varying values of d_p/σ in Figure 3. First and foremost, in all cases, the effect of feedback correction is to increase the relative velocity, and thereby increase the force estimation to the true value. The difference between the two formulations is important only at small values of Re_σ and for large particle size, because the feedback correction is negligible at large Reynolds numbers and particles much smaller than the filter width. At small and modest particle Reynolds numbers, even for particles as small as $d_p/\sigma = 0.1$, feedback correction is of importance, without which the force on the particle will be under-predicted.

4 Quasi-Steady Correction with Boundary Effect

We plan to implement the effect of a nearby wall with the help of a mirror particle. In order to evaluate the perturbation of the mirror particle at the real particle, we must evaluate velocity perturbation of the mirror particle at a point away from the center of mirror particle. In recognition of this fact, before we proceed to define the wall and the wall effect, let us first revisit the Oseen problem and obtain a more general solution.

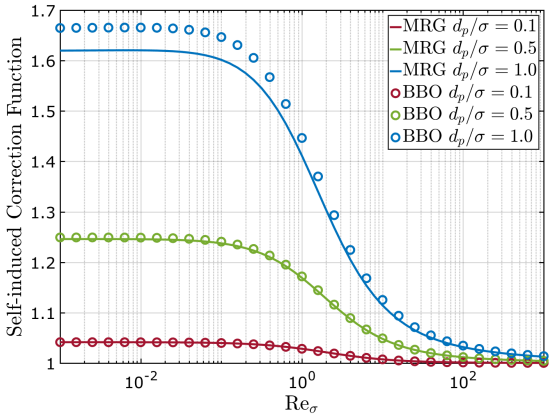

Figure 3: Self-induced correction function plotted against Re_σ for three different values of d_p/σ. The lines are for finite-Re_σ MRG equation and the symbols are for finite-Re_σ BBO equation.

4.1 Analytical Solution of the General Oseen Problem

Let us now consider the governing equations given in (12), but with all three components of the feedback force. As a result, the third term on the right hand side of (12) becomes $-(F'_x\mathbf{e}_x + F'_y\mathbf{e}_y + F'_y\mathbf{e}_z)\,G(\mathbf{x})$. In the analysis of the previous section, we sought the Oseen solution $\phi_{1c}\mathbf{u}'_{1c}$ only at the origin, since the self-induced perturbation was needed to be evaluated only at the origin, where the reference particle is located. However, in the present analysis, we require the Oseen solution $\phi_{1c}\mathbf{u}'_{1c}$ over the upper-half of the $x-y$ plane, namely the $\varphi = 0$ semi-infinite plane in the spherical coordinates, which is sufficient to account for the fact that the reference particle is located away from the mirror particle. In evaluating the perturbation effect of the mirror particle, we will place the mirror particle at the origin and the center of the reference particle to be on the upper $x-y$ plane denoted by the radial distance $0 \le l \le \infty$ and the angle $0 \le \alpha \le \pi$ from the positive x-axis. In this configuration, we recognize the fact that the force on the mirror particle can be oriented in any direction and thus will have all three components.

The details of obtaining the analytic solution of the Oseen equation in spectral space are presented in the Appendix A. We are interested in obtaining the volume-corrected perturbation flow averaged over the surface of a sphere of diameter d_p centered around any point located on the upper-half of $x-y$ place. This surface average is denoted as $\overline{\phi_{1c}\mathbf{u}'_{1c}}^{rs}$, where the superscript rs indicates that the spherical surface is centered about $\mathbf{r}$. The surface average can be approximated as

$$\overline{\phi_{1c}\mathbf{u}'_{1c}}^{rs} \approx \left[\phi_{1c}\mathbf{u}'_{1c}\right]_{\mathbf{r}} + \frac{d_p^2}{24}\left[\nabla^2\left(\phi_{1c}\mathbf{u}'_{1c}\right)\right]_{\mathbf{r}}, \tag{22}$$

where the two terms on the right denoted by $[\cdot]_{\mathbf{r}}$ are evaluated at the point $\mathbf{r}$ that is restricted to be on the upper $x-y$ plane. Converting the non-dimensional results of the Appendix A into dimensional terms we obtain the result

$$\overline{\phi_{1c}\mathbf{u}'_{1c}}^{rs} = -\frac{1}{6\pi\mu\sigma}\sqrt{\frac{2}{\pi}}\begin{bmatrix} \Psi_{xx\text{-}ef}(\mathbf{r}) & \Psi_{xy\text{-}ef}(\mathbf{r}) & 0 \\ \Psi_{yx\text{-}ef}(\mathbf{r}) & \Psi_{yy\text{-}ef}(\mathbf{r}) & 0 \\ 0 & 0 & \Psi_{zz\text{-}ef}(\mathbf{r}) \end{bmatrix}\mathbf{F}'. \tag{23}$$

where $\Psi_{ef}(\mathbf{r}) = \Psi_{os}(\mathbf{r}) - \dfrac{d_p^2}{24}\Psi_{Lap}(\mathbf{r})$. Ψ_{ef} is a tensor function of $\mathbf{r}$ and all nine components are in general non-zero. When $\mathbf{r}$ is restricted to be on the upper $x-y$ plane, it reduces to five non-zero components. In the limit $\mathbf{r} = 0$, the off-diagonal terms are zero and we revert to the simple vectorial form given in the previous section. Therefore we have the relations: $\Psi_{xx\text{-}ef}(\mathbf{r}=0) = \Psi_{x\text{-}ef}$, $\Psi_{yy\text{-}ef}(\mathbf{r}=0) = \Psi_{y\text{-}ef}$, and $\Psi_{zz\text{-}ef}(\mathbf{r}=0) = \Psi_{z\text{-}ef}$.

The above correction functions are the solutions to the Oseen equation and therefore can be correctly termed as non-dimensional *regularized Oseenlet*. An Oseenlet is the flow induced by a point force and it is singular at the origin.

In comparison, a regularized Oseenlet is the flow induced by a Gaussian smoothened point force and therefore it is regular over the entire domain. The vector $\{\Psi_{xx\text{-}os}, \Psi_{yx\text{-}os}, \Psi_{zx\text{-}os}\}^T$ can be interpreted as the *streamwise regularized Oseenlet*, where the Gaussian forcing is aligned with the ambient uniform flow along the x-direction. This solution is axisymmetric about the x-axis. Examples of this streamwise regularized Oseenlet are presented in Balachandar *et al.* [5]. In the limit of large Re_σ, the flow behaves like a narrow jet issuing from a small orifice located upstream of the origin, with a radial inward flow towards the origin outside of the jet. Far from the origin, the solution is well approximated by the Landau–Squires self-similar solution of a point momentum source [7]. In the other limit of small Re_σ, the flow away from the origin approaches the Stokes flow over a moving sphere. Near the origin, where we are interested in the perturbation flow, the departure from Landau-Squires solution is significant, due to the difference between a singular delta function forcing and a Gaussian forcing.

The vector $\{\Psi_{xy\text{-}os}, \Psi_{yy\text{-}os}, \Psi_{zy\text{-}os}\}^T$ can be interpreted as a *transverse regularized Oseenlet*, where the Gaussian forcing is in the y-direction, while the ambient uniform flow is along the x-direction. Similarly, the vector $\{\Psi_{xz\text{-}os}, \Psi_{yz\text{-}os}, \Psi_{zz\text{-}os}\}^T$ is a transverse regularized Oseenlet, where the Gaussian forcing is in the z-direction. The solution for the z-forcing can be easily obtained from that of the y-forcing, and unlike the streamwise regularized Oseenlet, these transverse regularized Oseenlets are not axisymmetric. However, as indicated in (23), on the $x-y$ plane, the solution of the y-forcing has only x and y velocity components, while the solution of the z-forcing has only the z velocity. The above interpretations extend to the Laplacian of the streamwise and transverse regularized Oseenlets as well.

The top half of Figure 4 shows the normalized axisymmetric function $\Psi_{xx\text{-}os}/\Psi_{x\text{-}os}$. The streamwise regularized Oseenlets are plotted for $\mathrm{Re}_\sigma = 0$, 1, and 100. The corresponding result of the normalized Laplacian function $\Psi_{xx\text{-}Lap}/\Psi_{x\text{-}Lap}$ is plotted in the bottom half of the figure. In both cases the contours are plotted on the upper half of the $x-y$ plane for a radial distance of up to 20σ. In the Stokes limit of $\mathrm{Re}_\sigma = 0$, there is an exact solution to the Gaussian Stokeslet given in Maxey and Patel [30] (also see [28]). In the present variables, this solution can be expressed as

$$\Psi_{ij\text{-}os}(\mathbf{r}) = A(r)\delta_{ij} + B(r)x_i, x_j\,, \tag{24}$$

where $r = |\mathbf{r}|$ and

$$\begin{aligned} A(r) &= \sqrt{\frac{\pi}{2}}\frac{3\sigma}{4r}\left[\left(1+\frac{\sigma^2}{r^2}\right)\mathrm{erf}\left(\frac{r}{\sqrt{2}\sigma}\right) - \frac{2\sigma}{\sqrt{2\pi}r}\exp\left(-\frac{r^2}{2\sigma^2}\right)\right] \\ B(r) &= \sqrt{\frac{\pi}{2}}\frac{3\sigma}{4r^3}\left[\left(1-\frac{3\sigma^2}{r^2}\right)\mathrm{erf}\left(\frac{r}{\sqrt{2}\sigma}\right) + \frac{6\sigma}{\sqrt{2\pi}r}\exp\left(-\frac{r^2}{2\sigma^2}\right)\right]. \end{aligned} \tag{25}$$

Thus, in the zero Re_σ limit, the solutions have a perfect left-right symmetry. At higher Re_σ, the left-right symmetry is lost and the flow takes a focused jet-like structure as predicted by the Landau-Squires flow. As a result of this jet-like structure, with increasing Re_σ the influence of the Gaussian forcing extends farther in the wake, while it remains contained within $r < 15\sigma$ in the case of zero Reynolds number. The Laplacian functions are structurally similar to the regularized Oseenlet, although the Laplacian decays at a faster rate with increasing r. From the color bar of the figure, it can be noted that at $r = 15\sigma$ the gray contour of $\Psi_{xx\text{-}os}/\Psi_{x\text{-}os}$ corresponds to a small non-zero value, while in case of $\Psi_{xx\text{-}Lap}/\Psi_{x\text{-}Lap}$, even at $r = 5\sigma$ the light blue contour indicates near zero value. Nevertheless, these functions are perfectly axisymmetric about the x-axis and therefore Figure 4 is sufficient for their complete construction.

The y-velocity of the streamwise regularized Oseenlet $\Psi_{yx\text{-}os}/\Psi_{x\text{-}os}$ and its Laplacian $\Psi_{yx\text{-}Lap}/\Psi_{x\text{-}Lap}$ are also axisymmetric functions. In contrast, the x-velocity of the transverse regularized Oseenlet $\Psi_{xy\text{-}os}/\Psi_{x\text{-}os}$ and its Laplacian $\Psi_{xy\text{-}Lap}/\Psi_{x\text{-}Lap}$ are not axisymmetric functions. Nevertheless, on the $x-y$-plane these two pairs of functions are identical $\Psi_{xy\text{-}os} = \Psi_{yx\text{-}os}$ and $\Psi_{xy\text{-}Lap} = \Psi_{yx\text{-}Lap}$. I.e., y-velocity of the streamwise regularized Oseenlet is the same as the x-velocity of the transverse regularized Oseenlet. Figure 5 shows $\Psi_{yx\text{-}os}/\Psi_{x\text{-}os}$ or $\Psi_{xy\text{-}os}/\Psi_{x\text{-}os}$ plotted on the upper-half of the $x-y$ plane. At $\mathrm{Re}_\sigma \to 0$, for the streamwise regularized Oseenlet there is left-right antisymmetry, with inward flow upstream and outward flow downstream. With increasing Re_σ the flow is increasingly dominated by an inward flow, which arises as a result of the strong streamwise oriented jet. Compared to the streamwise component of velocity presented in Figure 4, in Figure 5 the magnitude of transverse velocity is an order of magnitude lower. It should be noted that all the functions are appropriately normalized by $\Psi_{x\text{-}os}$ or $\Psi_{x\text{-}Lap}$, whose variations were earlier shown in 2. Thus, although the correction functions are $O(1)$ when scaled as shown in the plots, their unscaled values are substantially lower with increasing Re_σ.

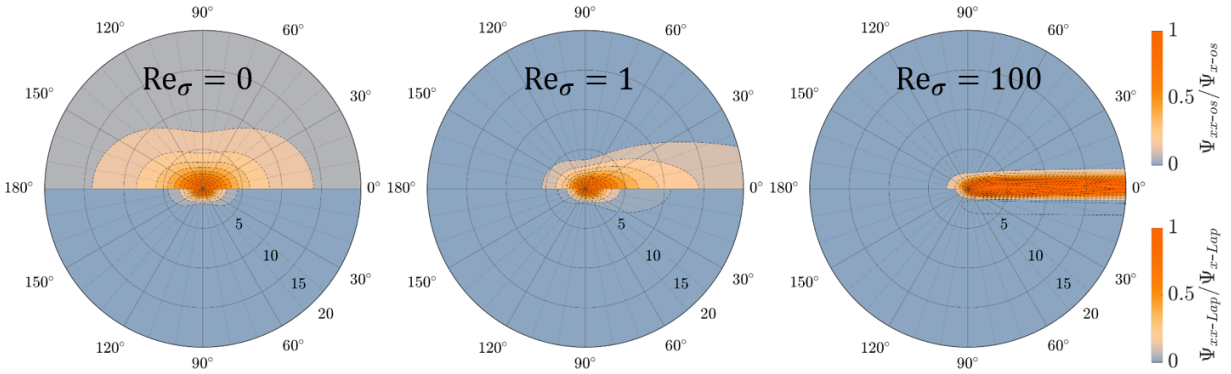

Figure 4: Contour plots of $\Psi_{xx\text{-}os}/\Psi_{x\text{-}os}$ presented as a function of $\mathbf{r}$ in the upper-half $x-y$ plane. Results are plotted for three different Re_σ. Also plotted in the bottom half of the picture are $\Psi_{xx\text{-}Lap}/\Psi_{x\text{-}Lap}$.

The normalized functions $\Psi_{yy\text{-}os}/\Psi_{y\text{-}os}$ and its Laplacian $\Psi_{yy\text{-}Lap}/\Psi_{y\text{-}Lap}$ are plotted in Figure 6. At $\mathrm{Re}_\sigma \to 0$, this flow is nothing but that shown for x-forcing rotated 90° about the z-axis. This however is not true at finite Re_σ. With increasing Reynolds number, the wake still tends to tilt towards the flow direction (i.e., along the positive x direction). However, since the force is along the y-direction, the x-tilt of the flow is not as strong as the Landau-Squires jet. The above observations apply for the Laplacian fields shown in the bottom half of the frames, although the Laplacian fields decay faster with increasing r.

Finally, the normalized functions $\Psi_{zz\text{-}os}/\Psi_{z\text{-}os}$ and $\Psi_{zz\text{-}os}/\Psi_{z\text{-}os}$ are plotted in Figure 7. In this case, the forcing is in the z-direction. Interestingly, at all Re_σ the resulting flow on the $x-y$ plane has only the z-component of velocity. At $\mathrm{Re}_\sigma \to 0$, the z-velocity contours are perfectly circular and decay rapidly past 7.5σ. Again, with increasing Re_σ, the velocity contours begin to tilt towards the positive x direction because of the cross-flow.

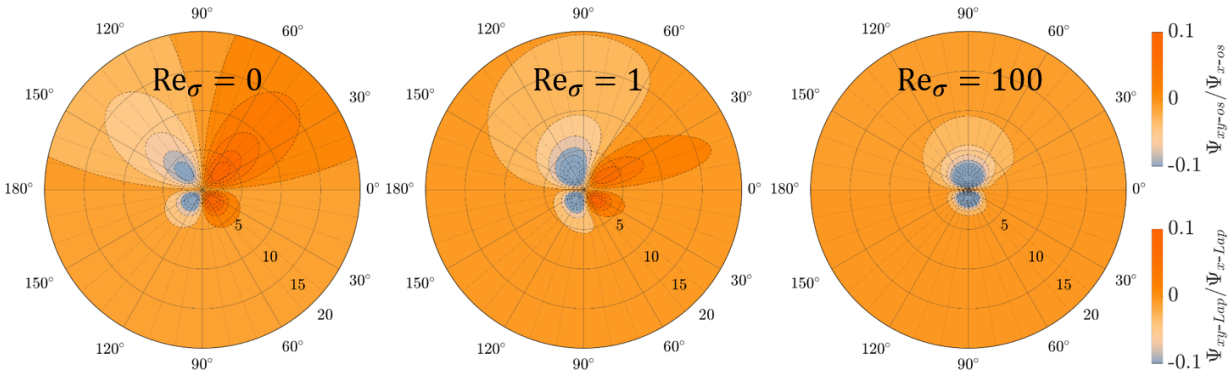

Figure 5: Contour plots of $\Psi_{yx\text{-}os}/\Psi_{x\text{-}os}$ presented as a function of $\mathbf{r}$ in the upper-half $x-y$ plane. Results are plotted for three different Re_σ. Also plotted in the bottom half of the picture are $\Psi_{yx\text{-}Lap}/\Psi_{x\text{-}Lap}$.

Figures 4 to 7 provide complete information on the analytically evaluated regularized Oseenlet obtained in Appendix A. The functions $\Psi_{xx\text{-}os}$, $\Psi_{yx\text{-}os}$, $\Psi_{yy\text{-}os}$, and $\Psi_{zz\text{-}os}$ and their Laplacian counterparts shown above are appropriate for Gaussian spreading of the feedback force. When grid resolution of the Gaussian forcing is fine enough, the

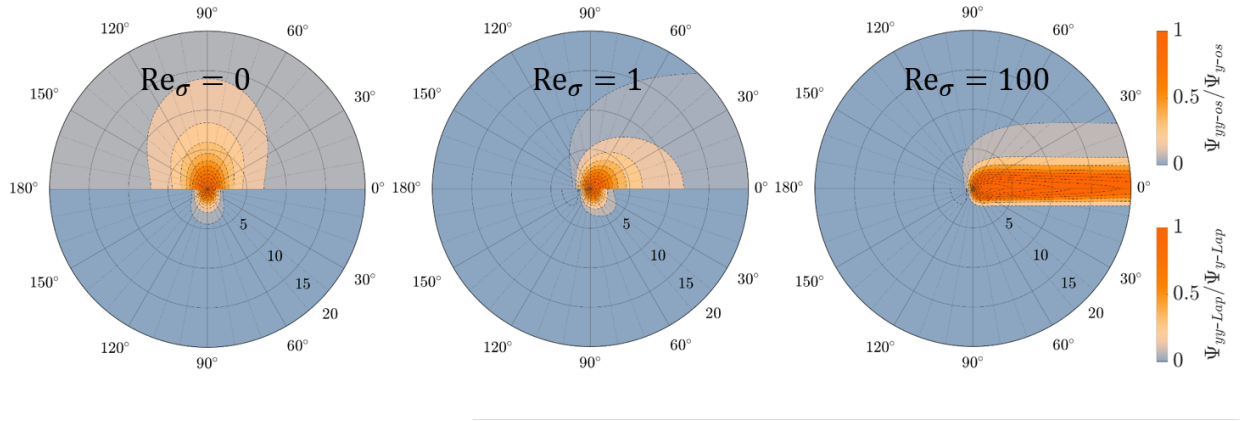

Figure 6: Contour plots of $\Psi_{yy\text{-}os}/\Psi_{y\text{-}os}$ presented as a function of $\mathbf{r}$ in the upper-half $x-y$ plane. Results are plotted for three different Re_σ. Also plotted in the bottom half of the picture are $\Psi_{yy\text{-}Lap}/\Psi_{y\text{-}Lap}$.

numerically evaluated regularized Oseenlet will correspond to that obtained analytically. If the numerical resolution is not sufficient, then the numerically obtained regularized Oseenlet functions will depart from their analytical form given above. This departure will mainly be quantitative, as we expect the functions to qualitatively remain the same. One may need to resort to numerical evaluation of the above functions on the $x-y$ plane in problems where the spreading function is not Gaussian or when numerical resolution is not adequate. The following simple algorithm can be followed to generate the numerical correction functions.

Algorithm-2a: Numerical Generation of Oseenlet Functions

1. This is a pre-processing step and therefore can be carried out once at the start of the simulation and stored as the eight two-dimensional functions suitably discretized on the $x-y$ plane.
2. Consider a large cuboidal domain whose sides are much larger than σ. Apply a uniform flow of unit non-dimensional magnitude along the x-direction. Apply appropriate inflow-outflow boundary conditions on the computational domain. Avoid using periodic boundary condition along the flow direction (i.e., along the x-direction). As we will see later in Section 6, this slows convergence.
3. In the first problem, apply a unit force along the x-direction with the spreading function of your choice centered about the center of the computational domain. Solve the Oseen governing equation (i.e., no need to use the full nonlinearity, since x, y, and z forces are being linearly superposed). Obtain the steady solution. The x and y components of perturbation velocity, appropriately scaled as given in (23), on the $x-y$ plane give $\Psi_{xx\text{-}os}$ and $\Psi_{yx\text{-}os}$. The Laplacian of this velocity on the $x-y$ plane gives $\Psi_{xx\text{-}Lap}$ and $\Psi_{yx\text{-}Lap}$.
4. In the second problem, apply a unit force along the y-direction with the chosen spreading function centered about the center of the computational domain. Solve the Oseen governing equation to obtain the steady solution. The y component of perturbation velocity when appropriately scaled is $\Psi_{yy\text{-}os}$. Also calculate and store the Laplacian.
5. In the third problem, apply a unit force along the z-direction with the chosen spreading function. Compute and store $\Psi_{zz\text{-}os}$ and $\Psi_{zz\text{-}Lap}$ on the $x-y$ plane.
6. Repeat the above three steps for different Re_σ.

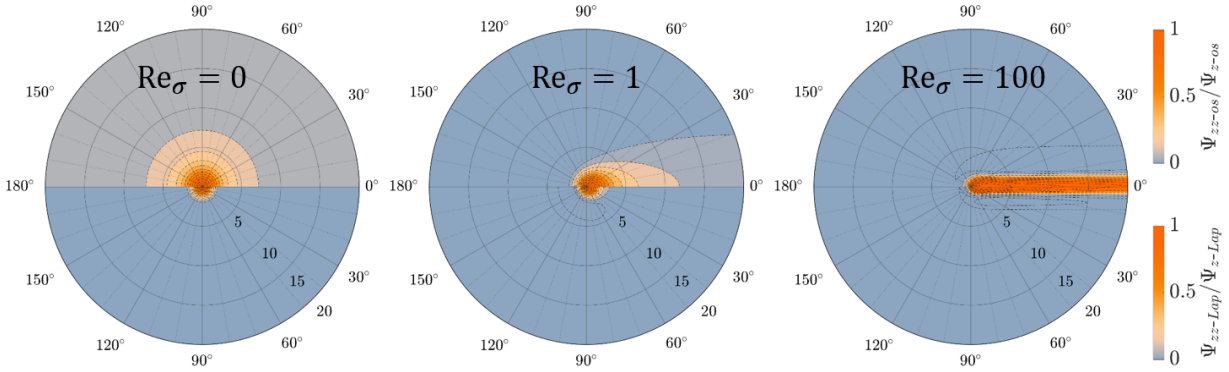

Figure 7: Contour plots of $\Psi_{zz\text{-}os}/\Psi_{z\text{-}os}$ presented as a function of $\mathbf{r}$ in the upper-half $x-y$ plane. Results are plotted for three different Re_σ. Also plotted in the bottom half of the picture are $\Psi_{zz\text{-}Lap}/\Psi_{z\text{-}Lap}$.

4.2 Vectorial Wall Correction

We now consider modification to the correction procedure when the particle is near a boundary. It is well known that in the Stokes limit, the drag on a particle increases for the same relative velocity when it is located close to a boundary [18; 19]. In the presence of a boundary, the particle also experiences shear, translation and rotation induced lift forces [24]. The enhanced drag and lift forces persist even at finite particle Reynolds number [25; 37; 38]. We anticipate self-induced correction to increase as well when a particle is located close to a boundary. As a result, recent self-induced correction procedures have also included the effect of boundaries [9; 31; 32]. In fact, it can be expected that self-induced correction is more important near a boundary than in the interior, because of the fact that grid size typically decreases near a boundary and as a result the particle may be comparable in size to the grid in the near-wall region, even when it is much smaller than the grid in the interior of the computational domain.

We approach the correction problem in the presence of a nearby wall with the following approximation. Consider a particle whose true relative fluid velocity to be $U_r\mathbf{e}_r$. Let a nearby flat wall be located at a distance $l/2$ from the center of the particle and let the outward unit normal (i.e., normal to the wall pointing away from the fluid region) be oriented as $\mathbf{e}_w$ (see the schematic shown in Figure 8). When $\mathbf{e}_r$ and $\mathbf{e}_w$ point in the same direction, the relative fluid velocity at the reference particle is directed towards the wall. In fact, this configuration must be understood as the particle moving directly away from the wall, so that in the frame attached to the particle, the fluid and the wall are moving to the right.

When $\mathbf{e}_r$ is orthogonal to $\mathbf{e}_w$, the fluid relative to the particle is moving parallel to the wall. The configuration where $\mathbf{e}_r$ is directed opposite to $\mathbf{e}_w$ corresponds to the particle moving towards the wall.

In the frame attached to the particle, the wall and fluid close to the wall are approaching the particle. Let the feedback force on the fluid by the reference particle be $-\mathbf{F}'$. As discussed before, part of the feedback force is due to quasi-steady force, which is oriented in the direction of relative velocity, and part of the feedback is from other mechanisms whose orientation is not limited to the direction of relative velocity. In general, the hydrodynamic force will have all three components.

We seek an Oseen solution to this problem with the inviscid effects of the wall approximated as a mirror image particle located on the other side of the wall. This approximation is also well-suited for the Gaussian feedback force projection in two-way coupled Euler-Lagrange situations due to the symmetric nature of slip wall boundary conditions. The following three pieces of information characterize the image particle: (i) Its center is located at $-l\mathbf{e}_w$ from the reference particle. (ii) The relative velocity $U_r\mathbf{e}_r$ at the reference particle becomes $U_r\mathbf{e}_{rI}$ at the image where $\mathbf{e}_{rI} = \mathbf{e}_r - 2(\mathbf{e}_r \cdot \mathbf{e}_w)\mathbf{e}_w$. This has the effect of keeping the wall-parallel component of velocity the same, while changing the direction of the wall-normal component. (iii) The feedback force at the image particle is given by $-\mathbf{F}'_I = -\mathbf{F}' + 2(\mathbf{F}' \cdot \mathbf{e}_w)\mathbf{e}_w$, which also has the effect of keeping the wall-parallel component the same, while

reversing the direction of the wall-normal component. For later use, the calculation of the image force can also be expressed as a transformation operator as $-\mathbf{F}'_I = -\mathbf{T}_F\mathbf{F}'$, where the 3×3 matrix $\mathbf{T}_F$ will transform the feedback force of the reference particle to the feedback force of the image.

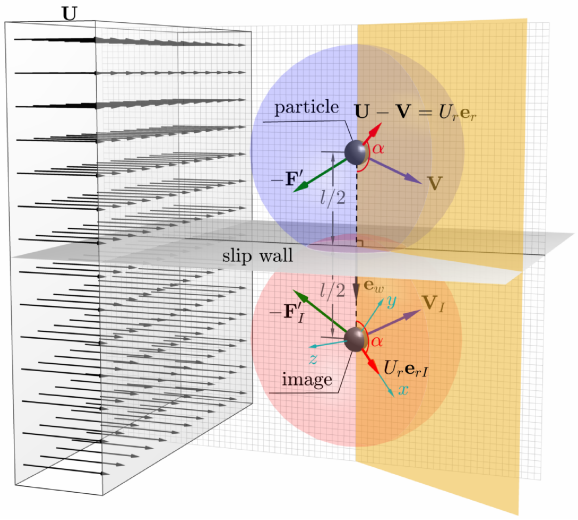

Figure 8: Schematic of the interaction between a particle and a nearby wall. The feedback force on the particle is denoted by the blue arrow that can have nonzero components on each axis. The blue transparent sphere is the iso-surface of the half-width of the Gaussian feedback force. The image particle and its reflected feedback force are shown as well. The additional effect on the real particle from the mirror image can be evaluated by Equation (23) in the frame of the cyan coordinates attached to the image particle, whose x axis is aligned with $\mathbf{e}_{rI}$ and y axis is on the plane formed by $\mathbf{e}_{rI}$ and $\mathbf{e}_w$ (yellow transparent plane). α is the angle between $\mathbf{e}_{rI}$ and $\mathbf{e}_w$, or $\mathbf{e}_r$ and $-\mathbf{e}_w$.

We again consider the separation of the feedback force given in (11) into quasi-steady and other components. Furthermore, we make the important assumption that the self-induced perturbation velocity at the reference particle is the sum of its own velocity correction and that due to the image particle. Analogous to (16) the velocity correction can be expressed as

$$\begin{aligned}\overline{\phi_{1c}\mathbf{u}'_{1c}}^{s} &\approx -\frac{1}{6\pi\,\mu\sigma}\sqrt{\frac{2}{\pi}}\mathbf{M}^T\,\mathbf{B}_0\,\mathbf{M}\,\left(\mathbf{F}'_{qs}+\mathbf{F}'_{ot}\right) - \frac{1}{6\pi\,\mu\sigma}\sqrt{\frac{2}{\pi}}\mathbf{M}_I^T\,\mathbf{B}(\mathbf{M}_I\mathbf{r}_{ir})\,\mathbf{M}_I\,\left(\mathbf{F}'_{qs,I}+\mathbf{F}'_{ot,I}\right)\\ &\approx -\frac{1}{6\pi\,\mu\sigma}\sqrt{\frac{2}{\pi}}\underbrace{\left(\mathbf{M}^T\,\mathbf{B}_0\,\mathbf{M}+\mathbf{M}_I^T\,\mathbf{B}(\mathbf{M}_I\mathbf{r}_{ir})\,\mathbf{M}_I\mathbf{T}_F\right)}_{=\mathbf{C}}\,\left(\mathbf{F}'_{qs}+\mathbf{F}'_{ot}\right)\,,\end{aligned} \tag{26}$$

where the unitary rotation matrix $\mathbf{M}$ and the scaling matrix $\mathbf{B}_0$ are the same as those given in (17). Thus, the first term on the right hand side is the same term as before in the absence of the wall. The second term on the right hand side accounts for the effect of the image where the unitary rotation matrix $\mathbf{M}_I$ and the scaling matrix $\mathbf{B}(\mathbf{M}_I\mathbf{r}_{ir})$ are given as

$$\mathbf{M}_I = \begin{bmatrix} \leftarrow & \mathbf{a}_I & \rightarrow \\ \leftarrow & \mathbf{b}_I & \rightarrow \\ \leftarrow & \mathbf{c}_I & \rightarrow \end{bmatrix},\ \mathbf{B}(\mathbf{M}_I\mathbf{r}_{ir}) = \begin{bmatrix} \Psi_{xx\text{-}ef}(\mathbf{M}_I\mathbf{r}_{ir}) & \Psi_{xy\text{-}ef}(\mathbf{M}_I\mathbf{r}_{ir}) & 0 \\ \Psi_{yx\text{-}ef}(\mathbf{M}_I\mathbf{r}_{ir}) & \Psi_{yy\text{-}ef}(\mathbf{M}_I\mathbf{r}_{ir}) & 0 \\ 0 & 0 & \Psi_{zz\text{-}ef}(\mathbf{M}_I\mathbf{r}_{ir}) \end{bmatrix}. \tag{27}$$

In the above equation, $\mathbf{r}_{ir}$ corresponds to the vector from the center of the image particle to the center of the reference particle and it is given by

$$\mathbf{r}_{ir} = -l\mathbf{e}_w \tag{28}$$

In the unitary rotation matrix $\mathbf{M}$, $\mathbf{a}_I = \mathbf{e}_{rI}$ is the unit vector aligned along the relative velocity of the image particle, $\mathbf{b}_I$ is the unit vector that is normal to $\mathbf{a}_I$ and lies on the plane containing both the relative velocity and the separation vector $\mathbf{r}_{ir}$ and it is explicitly given as

$$\mathbf{b}_I = \frac{\mathbf{r}_{ir} - (\mathbf{r}_{ir} \cdot \mathbf{e}_{rI})\mathbf{e}_{rI}}{|\mathbf{r}_{ir} - (\mathbf{r}_{ir} \cdot \mathbf{e}_{rI})\mathbf{e}_{rI}|} \,. \tag{29}$$

The unit vector $\mathbf{c}_I = \mathbf{a}_I \times \mathbf{b}_I$ and thus normal to the other two. Note that in the lab coordinates $\mathbf{r}_{ir}$ will be arbitrarily oriented depending on the location of the particle and the orientation of the nearby wall. On the other hand, from the definition of the unitary matrix, $\mathbf{M}_I \mathbf{r}_{ir}$ is guaranteed to have components only in the first two coordinates. I.e., the arguments to the correction functions of the $\mathbf{B}$ matrix are on the $x - y$ plane in which these functions were earlier defined. Thus, in the second term $\mathbf{M}_I \left(\mathbf{F}'_{qs,I} + \mathbf{F}'_{ot,I}\right)$ projects the feedback force at the image to this coordinate system, where the perturbation velocity at the reference particle is evaluated with the multiplication of the $\mathbf{B}$ matrix, which then is brought back to the lab coordinate by left multiplying with $\mathbf{M}_I^T$.

A subtle point regarding ϕ_{1c} in (26) must be pointed out. With the influence of a nearby wall, ϕ_{1c} should correctly correspond to the volume fraction of the continuous phase in the presence of the particle located at the origin and its image located at a distance l away. But since the effect of volume fraction is quite small, the additional volume effect of the image particle is even smaller and can generally be ignored.

Substituting (26) and (5) into (6) we obtain the following vector form of the *wall corrected quasi-steady drag*

$$\mathbf{F}'_{qs} = \underbrace{\left[\mathbf{I} - \frac{d_p \Phi}{\sigma\sqrt{2\pi}}\mathbf{C}\right]^{-1}}_{\text{feedback correction}} \left[3\pi\mu d_p \left(\overline{\phi_{1c}\mathbf{u}_c}^s - \mathbf{V}\right)\Phi + \frac{d_p \Phi}{\sigma\sqrt{2\pi}}\mathbf{C}\,\mathbf{F}'_{ot}\right] , \tag{30}$$

where $\mathbf{I}$ is the 3×3 identity matrix and the operator $\mathbf{C}$ was defined in (26) as the sum of reference and image operators. In defining it we have used the relation $-\mathbf{F}'_I = -\mathbf{T}_F \mathbf{F}'$. It is to be noted that even in the absence of other forces represented by $\mathbf{F}'_{ot}$, a systematic correction procedure involving the wall effect needs to be vectorial. This is due to the fact that the reference particle will experience a wall-normal force due to the feedback force of its image, even when the true relative velocity is parallel to the wall. The correction procedure thus requires the inversion of a 3×3 matrix for each particle at each time step. However, this complication is required only when the distance from the wall is smaller than a few σ. For large values of l/σ, (30) becomes (18) and the implementation of the simpler form is sufficient. Equation (30) is certainly more complicated than the original one presented in (9). Nevertheless, we point out that it represents one of the simplest forms that consistently account for the wall effect and the effect of the other forces in the self-induced correction procedure. In fact, (30) incorporates some assumptions without which the correction process will become more complicated.

The above force expression along with (26) can be substituted back to obtain the following expression for the *true relative velocity*

$$\left(\overline{\mathbf{U}}^s - \mathbf{V}\right) = \underbrace{\left[\mathbf{I} - \frac{d_p \Phi}{\sigma\sqrt{2\pi}}\,\mathbf{C}\right]^{-1}}_{\text{feedback correction}} \left(\overline{\phi_{1c}\mathbf{u}_c}^s - \mathbf{V} + \frac{1}{6\pi\,\mu\sigma}\sqrt{\frac{2}{\pi}}\,\mathbf{C}\,\mathbf{F}'_{ot}\right) . \tag{31}$$

The feedback correction function is implicit in nature due to the dependence of Φ on Re and the matrix $\mathbf{C}$ on Re_σ. These two Reynolds numbers are defined in terms of the true relative velocity and they can be related to those computed in the EL simulation as shown below

$$\mathrm{Re} = \frac{|\overline{\mathbf{U}}^s - \mathbf{V}| d_p}{\nu} = \left| \left[\mathbf{I} - \frac{d_p \Phi}{\sigma\sqrt{2\pi}}\,\mathbf{C}\right]^{-1} \left(\mathrm{Re}_{EL}\,\mathbf{e}_{r,EL} + \frac{d_p}{6\pi\,\mu\sigma\nu}\sqrt{\frac{2}{\pi}}\,\mathbf{C}\,\mathbf{F}'_{ot}\right)\right| , \tag{32}$$

$$\mathrm{Re}_\sigma = \frac{|\overline{\mathbf{U}}^s - \mathbf{V}| \sigma}{\nu} = \left| \left[\mathbf{I} - \frac{d_p \Phi}{\sigma\sqrt{2\pi}}\,\mathbf{C}\right]^{-1} \left(\mathrm{Re}_{\sigma,EL}\,\mathbf{e}_{r,EL} + \frac{1}{6\pi\,\mu\nu}\sqrt{\frac{2}{\pi}}\,\mathbf{C}\,\mathbf{F}'_{ot}\right)\right| . \tag{33}$$

The above are implicit expressions for Re and Re_σ, which can be solved for any value of Re_{EL} computed in an EL simulation, with the additional information of d_p/σ and $\mathbf{F}'_{ot}$, the non-dimensional distance from the wall and the orientation of the wall with respect to relative velocity.

In summary, in the quasi-steady regime, the problem of self-induced velocity correction for a particle in the vicinity of a boundary can be stated as follows: Given the particle velocity $\mathbf{V}$, the local surface-averaged volume-corrected fluid velocity $\overline{\phi_{1c}\mathbf{u}_c}^s$, wall-normal distance l/σ, and wall orientation $\mathbf{e}_w$, along with other information such as d_p and ν, we want to calculate the correct quasi-steady force on the particle based on its true relative velocity. This evaluation can be achieved by pursuing the following steps:

Algorithm-2b: Quasi-steady Self-induced Velocity Correction Algorithm (close to a boundary)

1. As pre-processing step compute and store $\Psi_{xx\text{-}os}$, $\Psi_{xx\text{-}Lap}$ and all other regularized Oseenlet functions that are elements of $\mathbf{B}$ (see Algorithm-2a).
2. Compute the time-dependent quantity $\mathbf{F}'_{ot}$.
3. Compute the EL particle Reynolds number as $\mathrm{Re}_{EL} = |\overline{\phi_{1c}\mathbf{u}_c}^s - \mathbf{V}|d_p/\nu$ and the unitary vector $\mathbf{e}_{r,EL} = (\overline{\phi_{1c}\mathbf{u}_c}^s - \mathbf{V})/|\overline{\phi_{1c}\mathbf{u}_c}^s - \mathbf{V}|$.
4. Start the iteration with the initial assumption that the true relative velocity is the same as EL relative velocity. I.e., set $\mathrm{Re} = \mathrm{Re}_{EL}$, $\mathrm{Re}_\sigma = (\sigma/d_p)\,\mathrm{Re}_{EL}$, and $\mathbf{e}_r = \mathbf{e}_{r,EL}$.
5. Compute the values of $\mathbf{M}$, $\mathbf{M}_I$, $\mathbf{M}^T$, $\mathbf{M}_I^T$, $\mathbf{C}$, and Φ.
6. Apply the corrections given in (31) to calculate an improved estimate of the true relative velocity.
7. Use the updated true relative velocity to obtain improved estimates of Re, Re_σ, and $\mathbf{e}_r$.
8. Go back to step 5 and iterate till convergence.
9. Once converged, (36) to obtain the true quasi-steady force.

The above algorithm addresses the modification to the correction process when a particle gets close to a boundary. If a particle gets close to an edge of the domain (i.e., close to two boundaries) or close to a corner (i.e., close to three boundaries), the corresponding problems can be solved as well with three image particles in case of a nearby edge and seven image particles in case of a nearby corner. Accordingly, the matrix operator C can be easily defined as a sum of four contributions or eight contributions. The iterative nature of the algorithm presented above is examined in Appendix B, where it is shown that typically only three or four iterations are sufficient for adequate convergence.

5 An Approximate Unsteady Correction Procedure

In cases where the feedback force or the ambient condition varies fast enough, the self-induced velocity correction will not only depend on the instantaneous value of the feedback force, but also on its past history. Balachandar *et al.* [5] investigated the unsteady problem theoretically in the zero Reynolds number limit with a time-dependent Gaussian feedback force, and obtained an explicit integral equation for the self-induced velocity correction. This unsteady model was then extended to finite Reynolds number using numerical simulation results. Obtaining an Oseen solution in the unsteady regime with the wall effect taken into account is a challenging task. Instead, here we take a simple, but approximate, approach where we extend the findings of [5] to the present problem of vectorial correction with the inclusion of the wall effect. This is clearly an empirical approach, which can be improved upon in the future.

Based on the results of [5] the true relative velocity to the leading order can still be taken as the quasi-steady expression given by (31) and the unsteady effects appear as a convolution integral. This empirical expression for *true relative velocity* taking into account the unsteady effect can be expressed as

$$\begin{aligned}\left(\overline{\mathbf{U}}^s - \mathbf{V}\right) &= \left[\mathbf{I} - \hat{\mathbf{A}}\right]^{-1}\left(\overline{\phi_{1c}\mathbf{u}_c}^s - \mathbf{V} + \hat{\mathbf{B}}\,\mathbf{F}'_{ot}\right) \\ &\quad - \int_{-\infty}^{t} K(t-\tau;\mathrm{Re}_\sigma)\left[\frac{d}{dt}\left(\left[\mathbf{I} - \hat{\mathbf{A}}\right]^{-1}\left(\hat{\mathbf{A}}(\overline{\phi_{1c}\mathbf{u}_c}^s - \mathbf{V}) + \hat{\mathbf{B}}\,\mathbf{F}'_{ot}\right)\right)\right]_\tau d\tau\,,\end{aligned} \tag{34}$$

where we have used the substitution

$$\hat{\mathbf{A}} = \frac{d_p \Phi}{\sigma\sqrt{2\pi}}\mathbf{C} \quad \text{and} \quad \hat{\mathbf{B}} = \frac{1}{6\pi\,\mu\sigma}\sqrt{\frac{2}{\pi}}\mathbf{C}\,. \tag{35}$$

It should be noted that the term within the square parenthesis is evaluated at all past times and weighted by the exponentially decaying kernel K. As mentioned above in the quasi-steady procedure, the matrices $\hat{\mathbf{A}}$ and $\hat{\mathbf{B}}$ that appear in the first term on the right hand side of (34) must be based on the true relative velocity at time t and therefore must be iteratively determined. On the other hand, the matrices $\hat{\mathbf{A}}$ and $\hat{\mathbf{B}}$ that appear within the convolution integral in the second term on the right hand side are at the prior time τ, whose converged values from previous time steps can be stored and reused.

If we evaluate the convolution integral in an explicit manner using only previous time step values of the argument within the square parenthesis, the unsteady contribution can be taken as known in solving the implicit equation (34). The highlighted seven-step iterative procedure outlined for the quasi-steady correction can then be pursued even for unsteady correction. The only change is in step (6), where instead of (31) to calculate true relative velocity, we need to use (34). Once the true relative velocity is obtained, it can be used to calculate the *true unsteady wall-corrected quasi-steady force* as

$$\mathbf{F}'_{qs} = 3\pi\mu_f d_p \left(\overline{\mathbf{U}}^s - \mathbf{V}\right)\Phi\,. \tag{36}$$

For lack of better understanding, we will assume the kernel to be the same given in [6], which can be written as

$$K(t-\tau;\mathrm{Re}_\sigma) = \frac{1}{\sqrt{\exp\left(g\left(\dfrac{(t-\tau)|\overline{\mathbf{U}}^s - \mathbf{V}|}{\sigma}\right)\right) + \dfrac{2(t-\tau)\nu}{\sigma^2}}}\,, \tag{37}$$

where

$$g(\xi) = [1+\mathrm{erf}(\xi-8.08)](1.71+0.193\xi) + 0.4[1+\mathrm{erf}(8.08-\xi)]\xi\,. \tag{38}$$

The use of the above kernel in (34) assumes that the unsteady effect is not greatly modified by the presence of the boundary or by the presence of non-zero $\mathbf{F}'_{ot}$. In the absence of wall effects, when quasi-steady force is the only source of feedback, the results of [5] show that the above unsteady correction works well for a wide range of particle Stokes number in the context of a finite-Re free falling particle. Thus, we expect the above unsteady correction algorithm to perform well when the effects of nearby boundary and non-quasi-steady forces are not large. When these conditions are violated, the accuracy is likely to deteriorate. A more elaborate kernel that also depends on the parameters l/σ and α can be developed to improve the predictive capability when close to a boundary. Furthermore, if necessary, a different kernel to operate on the term $\hat{\mathbf{B}}\mathbf{F}'_{ot}$ can be attempted to account for the fact that the kernel given above was developed only for the case of quasi-steady force. These improvements are beyond the present scope.

Here we present an important principle: *One must correct only those aspects of two-way coupling included in an EL simulation*. Based on this principle, different variants of the correction procedure can be considered, which are displayed in Figure 9. (i) In a one-way coupled EL simulation, there is no need for any correction, since there is no self-induced perturbation. Particle force can be calculated based on EL fluid velocity at the particle location. (ii) If volume effect was ignored in a two-way coupled EL simulation, then the correction procedure must accordingly employ $\phi_{1c} = 1$, thus turning off the self-influence of particle volume. (iii) In an EL simulation, if the particle force was calculated without the Faxen correction (i.e., if the particle force was calculated using the BBO equation, instead of the MRG equation), then in equation (18), $\overline{\phi_{1c}\mathbf{u}_c}^s$ will be replaced by $[\phi_{1c}\mathbf{u}_c]_@$. Accordingly, in the correction procedure Ψ_{ef} should be replaced by Ψ_{os}, and thereby ignoring contribution from the Laplacian. (iv) In the case when forces other than quasi-steady are ignored, then the term involving $\mathbf{F}'_{ot}$ can be ignored in the implementation of the correction, which avoids the need for computing the unitary matrix away from the boundary. (v) Wall effects are needed only when a particle gets close to the wall (i.e., for $l/\sigma \lessapprox O(20)$). (vi) The results of [5] suggest that an unsteady correction is needed only when the Stokes number of the particle, defined as $\tau_p|\overline{\mathbf{U}}^s - \mathbf{v}|/\sigma$, is less than 5. Under this condition, the quasi-steady algorithm can be extended to include the convolution integral of past history to account for the unsteady effects.

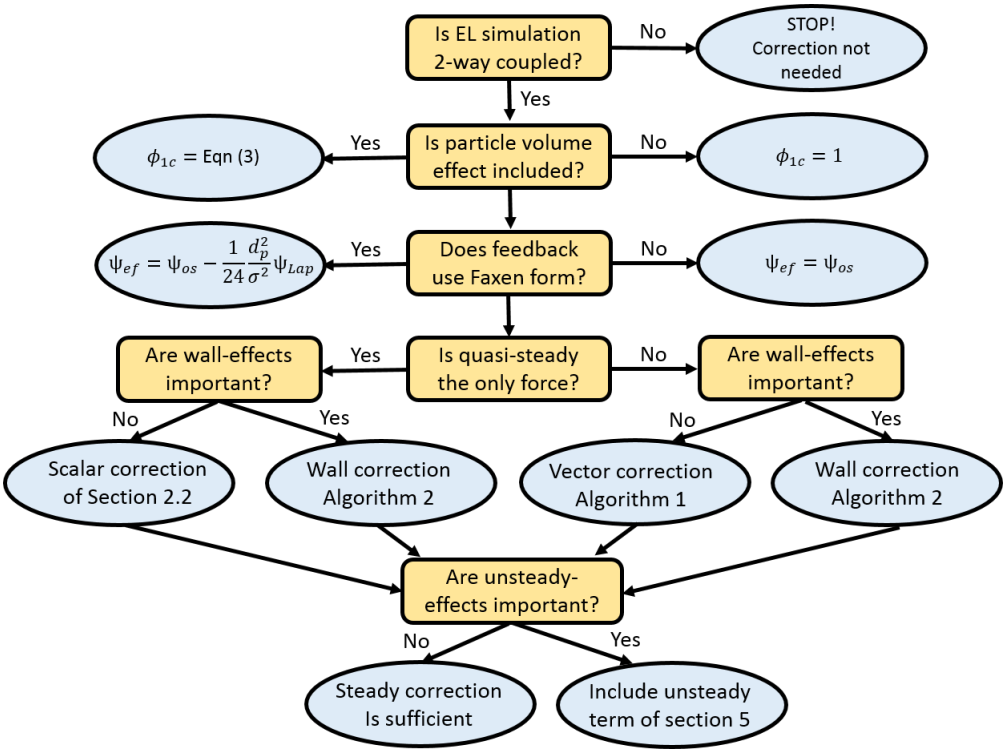

Figure 9: A flow chart showing decisions to be made in implementing the self-induced velocity correction procedure.

6 Effect of Numerical Methodology on Self-Induced Correction

By considering exact solutions of the Oseen equations using the Fourier transform technique, the above discussions have thus far avoided numerical issues. Numerical methodology employed in an EL simulation influences the above results on self-induced perturbation in three primary ways: (i) numerical simulations typically use a computational domain of finite size $\mathcal{L}$, as opposed to the unbounded domain of the theory, (ii) numerical simulations involve a finite grid resolution Δx, while the exact solution corresponds to the limit $\Delta x \to 0$, and (iii) in numerical simulations, the spatial derivatives are approximated with finite difference or compact difference schemes. It can be easily argued that in the limit $\mathcal{L} \gg \sigma$, the effect of finite size of the computational domain decreases, and in the limit $\Delta x \ll \sigma$, the effect of grid size becomes unimportant. In the limit $\Delta x \ll \sigma$, the error in numerically approximating the spatial derivatives also disappears. Thus, in the combined limits of $\mathcal{L} \gg \sigma$ and $\Delta x \ll \sigma$, the numerical correction procedure becomes nearly the same as the analytical correction procedure outlined in the prior sections. In practical implementations, we expect the condition $\mathcal{L} \gg \sigma$ to be reasonably valid, and thus in this section we are primarily concerned with the effect of the ratio $\Delta x/\sigma$ and the choice of spatial discretization.

We now resort to a discrete solution of the Oseen equation (12). The linear equations are again solved in the spectral domain by expanding the variables in 3D discrete Fourier transform, and the perturbation velocity and its Laplacian at the origin (i.e., at the reference particle) are then obtained with 3D discrete inverse Fourier transform. In the Fourier transform, the effects of computational domain size $\mathcal{L}$, the grid size Δx, and spatial discretization appear in the following manner: (i) The size of the computational domain dictates the smallest resolved wavenumber as $k_{min} = 2\pi/\mathcal{L}$. (ii) The size of the grid dictates the largest wave number according to Nyquist criterion as $k_{max} = \pi/\Delta x$. Since $\mathcal{L}/\Delta x = N$ gives the number of grid points along any coordinate direction, the corresponding wave numbers can be expressed as $k = 0, \pm k_{min}, \pm 2k_{min}, \cdots, \pm(N/2)k_{min}$, where the largest wave number is equal to $\pm k_{max}$. (iii) In Fourier space, the true first and second derivatives operators are multiplication by ιk and $-k^2$, respectively, whereas the numerical first and second derivatives become multiplication by modified wavenumber functions $\iota \tilde{k}$ and

$-\tilde{\tilde{k}}^2$, respectively, where the modified wavenumbers depend on the discretization scheme [2].

In case of spectral methods, the true wave numbers are preserved as

$$\tilde{k} = k \quad \text{and} \quad \tilde{\tilde{k}}^2 = k^2 \quad \text{for } k = 0, \pm k_{min}, \pm 2k_{min}, \cdots, \pm(N/2)k_{min}\,. \tag{39}$$

Whereas, in case of second-order central difference, the modified wavenumbers are

$$\tilde{k} = \frac{1}{\Delta x}\sin(k\Delta x) \quad \text{and} \quad \tilde{\tilde{k}}^2 = \frac{1}{\Delta x^2}\left[1-\cos(k\Delta x)\right] \quad \text{for } k = 0, \pm k_{min}, \pm 2k_{min}, \cdots, \pm(N/2)k_{min}\,. \tag{40}$$

It can be readily seen that in the low wavenumber (or long wavelength) limit of $k\Delta x \ll 1$, $\tilde{k} \approx k$ and $\tilde{\tilde{k}}^2 \approx k^2$ and thus the derivatives are accurate even in case of second-order central difference. However, in the high wavenumber limit of $k\Delta x \to \pi$, $\tilde{k}, \tilde{\tilde{k}}^2 \to 0$ and thus substantially deviate from the true values. Most importantly, self-perturbation correction of spatial discretizations, such as finite-difference, compact-difference, finite-volume or other methods, can be obtained in the present approach with the appropriate modified wavenumbers. The modified wavenumbers of higher-order finite-difference and compact-difference schemes can be found in [2].

From the solution of the Oseen equation, the streamwise and cross-stream perturbation velocities in spectral space can be obtained as

$$\begin{aligned}
\widehat{\phi_{1c}u'_{1c}} &= -\frac{F_x\ \mathrm{Re}_\sigma\left(1-\iota\dfrac{\mathrm{Re}_\sigma\,\tilde{k}_x}{|\tilde{\tilde{k}}|^2}\right)}{|\tilde{\tilde{k}}|^2\left(1+\dfrac{\mathrm{Re}_\sigma^2\,\tilde{k}^2}{|\tilde{\tilde{k}}|^4}\right)}\left(1-\frac{\tilde{k}_x\tilde{k}_x}{\tilde{k}_x^2+\tilde{k}_y^2+\tilde{k}_z^2}\right)\hat{G}\,,\\
\widehat{\phi_{1c}v'_{1c}} &= -\frac{F_y\ \mathrm{Re}_\sigma\left(1-\iota\dfrac{\mathrm{Re}_\sigma\,\tilde{k}_x}{|\tilde{\tilde{k}}|^2}\right)}{|\tilde{\tilde{k}}|^2\left(1+\dfrac{\mathrm{Re}_\sigma^2\,\tilde{k}^2}{|\tilde{\tilde{k}}|^4}\right)}\left(1-\frac{\tilde{k}_y\tilde{k}_y}{\tilde{k}_x^2+\tilde{k}_y^2+\tilde{k}_z^2}\right)\hat{G}
\end{aligned} \tag{41}$$

for $k_x, k_y, k_z = \pm k_{min}, \pm 2k_{min}, \cdots, \pm(N/2)k_{min}$ (here the mean mode is ignored in order to reduce the effect of periodicity). In the above, we have used the notation $|\tilde{\tilde{k}}|^2 = \tilde{\tilde{k}}_x^2 + \tilde{\tilde{k}}_y^2 + \tilde{\tilde{k}}_z^2$. We now take the discrete inverse Fourier transform and evaluate at the center of the reference particle (i.e. at the origin) to obtain the following final results

$$[\phi_{1c}u'_{1c}]_@ = \sum_{k_x}\sum_{k_y}\sum_{k_z}\widehat{\phi_{1c}u'_{1c}} \quad \text{and} \quad \left[\nabla^2\phi_{1c}u'_{1c}\right]_@ = \sum_{k_x}\sum_{k_y}\sum_{k_z}-(\tilde{\tilde{k}}_x^2+\tilde{\tilde{k}}_y^2+\tilde{\tilde{k}}_z^2)\widehat{\phi_{1c}u'_{1c}}\,. \tag{42}$$

These results are then recast into the following form to obtain the corresponding numerical Oseen and Laplace functions

$$\overline{\phi_{1c}u'_{1c}}^{s} \approx [\phi_{1c}u'_{1c}]_@ + \frac{d_p^2}{24}\left[\nabla^2(\phi_{1c}u'_{1c})\right]_@ = -\frac{F'_x}{6\pi\,\mu\sigma}\sqrt{\frac{2}{\pi}}\underbrace{\left[\Psi_{Nx\text{-}os} - \frac{1}{24}\frac{d_p^2}{\sigma^2}\Psi_{Nx\text{-}Lap}\right]}_{\Psi_{Nx\text{-}ef}}\,, \tag{43}$$

with similar expressions for $\overline{\phi_{1c}v'_{1c}}^{s}$. We have included "$N$" in the subscript to denote that these correspond to numerical implementation of the correction functions.

In all cases, for adequate convergence of computed $\overline{\phi_{1c}u'_{1c}}^{s}$ we require a very large computational box (i.e., $\mathcal{L}/\sigma \gg 1$). This need for a large domain increases with increasing Re_σ. This is due to the combined effects of the region of perturbation being very long along the streamwise direction at higher Re_σ and the use of periodic boundary conditions implicit in the discrete Fourier expansion. As illustrated by the numerical simulations of [5], with the use of inflow/outflow boundary conditions along the flow direction, the need for a very large domain can be avoided in an actual EL simulation. Figure 10 shows $\Psi_{Nx\text{-}os}$ plotted as functions Re_σ for $\Delta x/\sigma = 1$ and 2 for three different

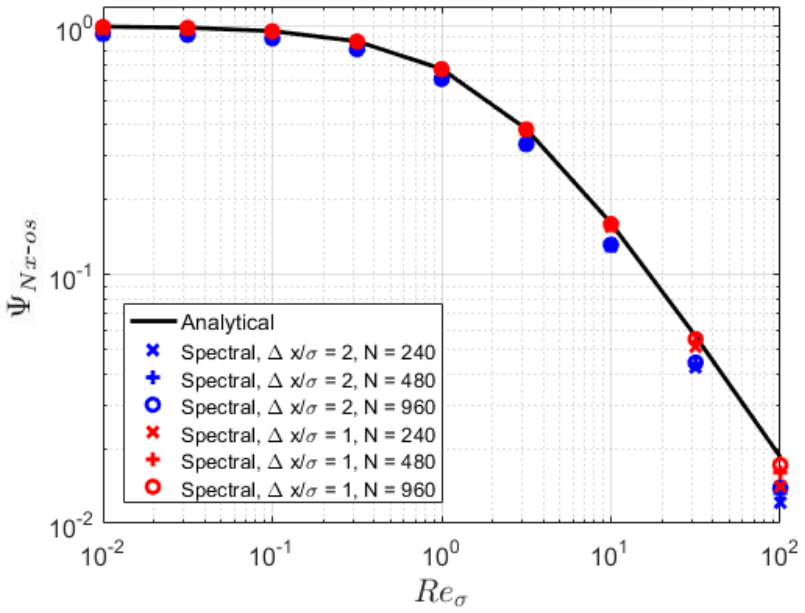

Figure 10: Plot of $\Psi_{Nx\text{-}os}$ for spectral methods at two different grid resolutions and three values of N.

uniform grids of $N = 240$, 480, and 960, whose domain size along the streamwise direction extends from $-N\Delta x/2$ to $N\Delta x/2$. Also plotted in the figure for reference is the analytical function Φ_{os} given in (14). For $\Delta x/\sigma = 1$, the results converge to the analytic solution for small values of $\mathrm{Re}_\sigma \lessapprox 1$. But a longer domain with more grid points is needed to converge to the analytic solution and the convergence is only algebraic due to the periodic nature of the Fourier expansion. Nevertheless, it can be seen that a grid resolution of $\Delta x = \sigma$ is sufficient to recover the analytical behavior. There is noticeable difference for a coarser grid resolution of $\Delta x = 2\sigma$.

The ratio $\Psi_{Nx\text{-}os}/\Psi_{x\text{-}os}$ is presented in Figure 11 for the second-order central difference approximation. Again the results are presented for a sufficiently large domain, where convergence has been achieved. The results for three different grid resolutions of $\Delta x/\sigma = 1/2$, 1 and 2 are shown for a range of Re_σ. For $\Delta x/\sigma = 1/2$, it is clear that the error in employing the analytic function $\Psi_{x\text{-}os}$ is less than 2%. This is consistent with [23]'s recommendation that $\Delta x/\sigma \leq \sqrt{2\ln 2}$ for adequate resolution of the Gaussian regularization. Since second-order central difference is less accurate than other higher-order finite and compact difference schemes, we conclude that no special adjustment is needed and the analytical correction procedure can be implemented in a wide variety of numerical approaches, provided grid resolution Δx is smaller than $\sigma/2$.

7 Effect of Regularization or Spreading Function

The discussions of the above sections have all been based on Gaussian spreading function. But a number of other approaches to two-way coupling, including particle-in-cell approach [13], discrete delta function spreading [1; 35], and Wendland function smoothening [15] have been used by researchers. It is clear that correction procedure can be easily repeated to other spreading functions by using their Fourier transforms instead of that of the Gaussian in the Oseen analysis. In this section, as an example, we will consider two other spreading functions to illustrate that not only the correction procedure can be easily extended to these functions, but also that the results of the different spreading functions are quite similar.

To demonstrate the generality of the correction procedure, we consider the following three hyper-Gaussian spread-

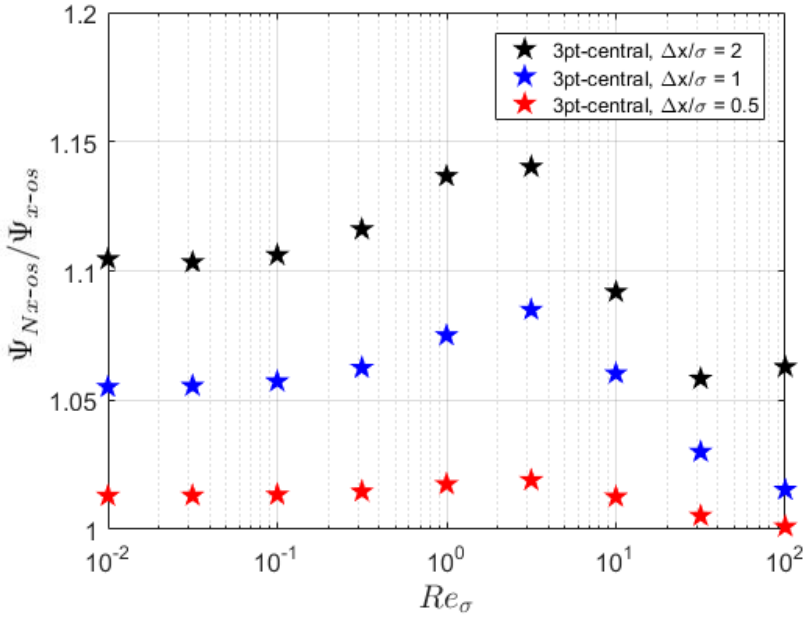

Figure 11: Plot of $\Psi_{Nx\text{-}os}/\Psi_{x\text{-}os}$ for three-point central difference scheme at three different grid resolutions.

ing functions:

$$G^1(r) = \frac{1}{(2\pi)^{3/2}\sigma^3}\exp\left(-\frac{r^2}{2\,\sigma^2}\right), \tag{44}$$

$$G^2(r) = \frac{1}{\pi\,\Gamma\left(\frac{3}{4}\right)(\ln 16)^{3/4}\,\sigma^3}\exp\left(-\frac{r^4}{\ln 16\,\sigma^4}\right), \tag{45}$$

$$G^3(r) = \frac{2^{5/8}}{\pi\,\Gamma\left(\frac{3}{8}\right)(\ln 4)^{9/8}\,\sigma^3}\exp\left[-\frac{r^8}{2(\ln 4)^3\,\sigma^8}\right], \tag{46}$$

where r is the radial distance in a three-dimensional domain. All three functions have been properly normalized, so that their 3D volumetric integral is unity. Also, they have been defined such that their half-widths are identical at $r = \sqrt{2\ln 2}\,\sigma$. The inset in Figure 12 shows the three hyper-Gaussian functions plotted as a function of r, where the half-width (the point where the functions reach half the peak value) is marked. It can be observed that going from G^1 to G^3 the function gradually evolves from the standard Gaussian to a top-hat-like shape. Thus, the results for G^3 can be taken to resemble that of a smoothened PIC approach.

In the simplest scalar correction case, in which there is only the quasi-steady force and no wall effect, the self-induced velocity is in the form of $\overline{(\phi_{1c}u_{1c})}^s = -CF'_x\Psi_{x\text{-}os}/(3\pi\sqrt{2\pi}\mu\sigma)$. It should be noted that C is a constant and it is independent of F'_x or Re_σ. It will however vary for the different spreading (or regularization) functions. For example, for the standard Gaussian function $C^1 = 1$, while $C^2 = 3\pi/(8\,\Gamma(7/4)(\ln 2)^{1/4}) = 1.405$ and $C^3 = 1.538$. From this it can be readily seen that at small Re_σ the smoothing function G^2 requires a 40.5% higher correction and the PIC-like smoothing requires a 53.8% higher correction. Figure 12 shows plots of $\Psi_{x\text{-}os}$ versus Re_σ for the three spreading functions. It is clear that the decay rate is the same for all three cases. Furthermore, the magnitude of correction for the non-Gaussian spreading slightly increases at higher Re_σ. From these results it appears that the analytical correction functions are weakly dependent on the form of the spreading function. As a result, if the precise form of the correction function is not available for any spreading function, one can reasonably use the correction

functions given here at the price of some inaccuracy.

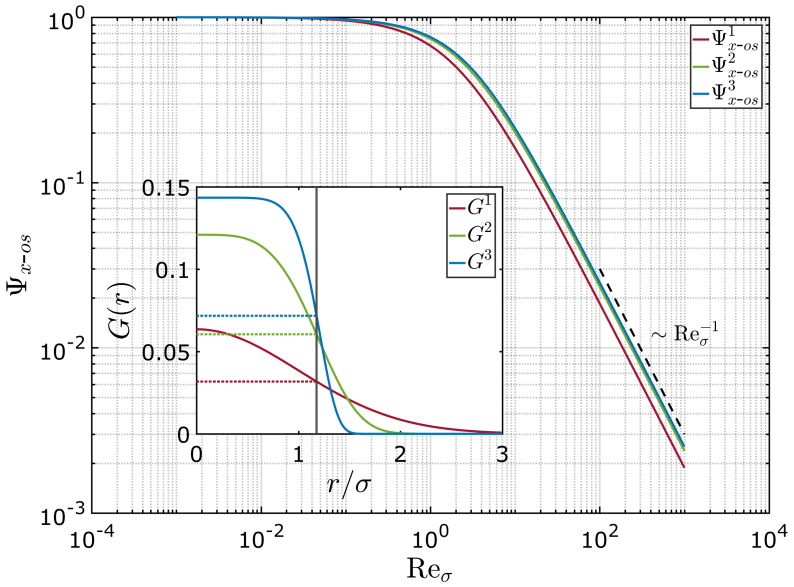

Figure 12: Plot of $\Psi_{x\text{-}os}$ for three different filter functions.

8 Numerical Validation of the Proposed Velocity Correction Algorithm

As simple tests of the self-induced velocity correction model developed in this work, we have performed two Euler-Lagrange simulation scenarios and used their results to validate the accuracy of the correction model. In the first case, a single particle of diameter d_p is fixed at the origin subjected to a uniform incompressible flow of magnitude U oriented along the x-direction. The particle diameter and the ambient flow velocity are chosen as the length and velocity scales. The hydrodynamic force exerted on the particle is of constant magnitude $\mathbf{F}' = 20\mu d_p|U|$. In order to test the vectorial version of the correction procedure, the direction of the hydrodynamic force is allowed to differ from the flow direction. Without loss of generality, the force direction was restricted to the $x-y$ plane and the angle with the x-axis, α was varied from 0 to π. A Gaussian filter of $\sigma/d_p = 2$ was used to spread the force back onto the flow. The two-way coupled Euler-Lagrange simulations were performed using the high-order spectral element method code Nek5000 with a grid resolution of $\Delta x/d_p = 10/12$ that is fine enough to resolve the Gaussian filter function as confirmed with a grid-independence study by comparing $\Delta x/d_p = [10/2, 10/4, 10/8, 10/12, 10/16]$ cases. Figure 13 shows detailed comparison between simulation results and model prediction. The simulated self-induced velocities converge well and remain unchanged for $\Delta x/d_p \leq 10/12$ in all cases. The model predicted values match converged simulation results, except for the streamwise self-induced velocity in the $\sigma/d_p = 8$ case (blue symbols) in Figure 13a. The difference, in this case, is due to the very broad spreading of the self-induced flow field which interacts with the boundary condition of the finite simulation domain.

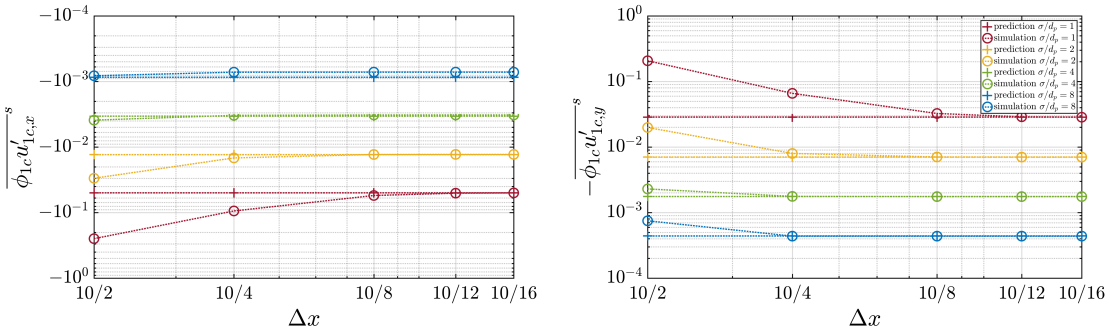

Figure 13: Detailed comparison of simulated (circle symbols) and predicted (plus symbols) results for the (a) streamwise and (b) spanwise self-induced velocity at the particle center. The x-axis represents the mean grid spacing in simulations. In all the four two-way coupled Euler-Lagrange cases, $\alpha = \pi/4$, $\mathrm{Re}_p = 10$, and $|\mathbf{F}'| = 1$.

Three different particle Reynolds numbers of $\mathrm{Re}_p = [0.1, 1, 10]$ were investigated and the results are shown in Figure 14, where the self-induced velocity that arises in the EL simulation (symbols) is compared against the model prediction (lines). The results for the streamwise (or x) velocity are shown in frame (a) and the corresponding results for the transverse (or y) velocity are shown in frame (b). The agreement is quite good at all values of Re_p. At the higher Reynolds numbers considered, the difference between the model prediction and the simulation result for the streamwise component slightly increases at $\alpha = 0$ and π. The prediction of the transverse velocity correction is quite good even at the higher Reynolds number. The results indicate that the present model can accurately predict self-induced velocity especially for $\mathrm{Re}_p \leq \mathcal{O}(10)$. The self-induced correction model corrects up to 40% error in point-particle drag for the smallest Reynolds number case considered, by properly accounting for the deviation between the true undisturbed incoming flow velocity and the flow velocity computed in an EL simulation.

The results shown in Figure 14 are for the self-induced perturbation velocity that has been averaged over the surface of the particle. This surface average has been calculated as the summation of the self-induced velocity and its Laplacian evaluated at the center of the particle as given in (13). We also investigated the accuracy of the correction model in evaluating both the self-induced velocity at the center of the particle and Laplacian separately. In all the cases considered, both the self-induced velocity and its Laplacian evaluated at the center of the particle were well predicted by the model quite accurately. The Laplacian was more than an order of magnitude smaller and therefore the correction procedure can be applied quite accurately based on only the correction velocity evaluated at the center of the particle.

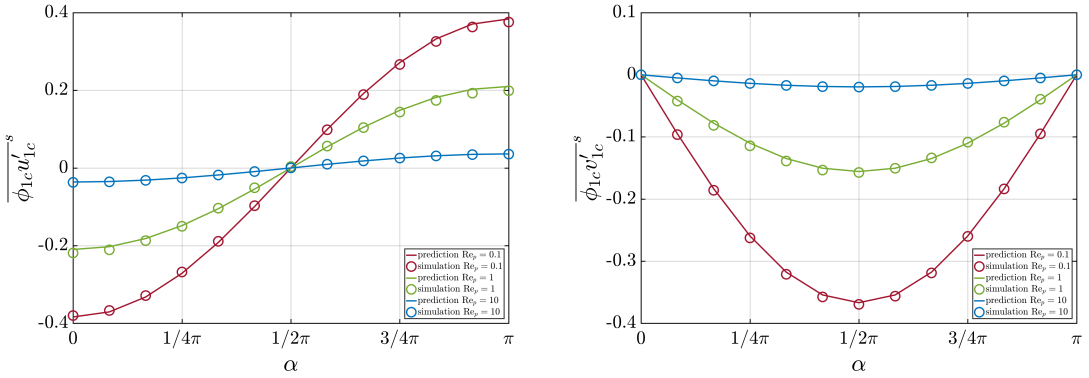

Figure 14: Self-induced velocity at the particle computed from simulation (symbols) and vectorial correction model presented in Algorithm-1 (lines) for varying orientations of the feedback force with respect to the ambient flow direction. Frame (a) presents the x component of self-induced velocity for $\mathrm{Re}_p = 0.1$, 1, and 10. Frame (b) presents the corresponding y component.

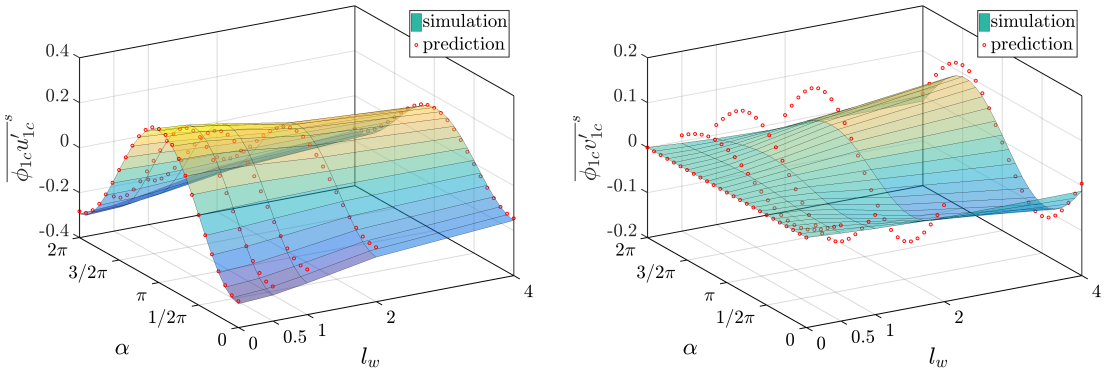

Figure 15: Self-induced velocity at the particle computed from simulation and the correction model presented in Algorithm-2b for varying orientations of the feedback force with respect to the ambient flow direction and for varying distances between the particle and the nearby wall. Frame (a) presents the x component of self-induced velocity for $\mathrm{Re}_p = 1$. Frame (b) presents the corresponding y component.

As the second numerical validation we consider evaluating the correction model with the inclusion of the effect of a nearby wall. The general setting is the same as the previous test case, except for the force magnitude is now $\mathbf{F}' = 10\mu d_p|U|$ and for the addition of an infinite wall that is parallel to the incoming flow velocity (i.e., in the EL simulations, the inviscid wall extends along the $x - z$ plane). The particle is again at the origin and the wall is given by the plane $y = -l_w$. We will only present the results for $\mathrm{Re}_p = 1$ as the results are similar at other Reynolds numbers. Figure 15 shows the streamwise and wall-normal velocity correction in the presence of the nearby wall. The self-induced velocity obtained from EL simulations and the corresponding value predicted by Algorithm-2b are shown as surfaces for varying particle-to-wall distance l_w and force orientation α relative to the x-axis along the $x - y$ plane. The results show that the present correction model is able to predict the self-induced velocity quite accurately for varying wall distances and for varying force orientations. The transverse correction is zero at $l_w = 0$, but the correction increases with increasing l_w. If we note that the results of Figure 14 correspond to the limit of the wall being far away, both the streamwise and transverse corrections can be expected to level off as $l_w \to \infty$. The model somewhat overestimates the correction velocity of the transverse component at intermediate values of l_w, but the overestimation decreases as $l_w \to \infty$ as can be observed in Figure 14. The largest difference between the simulation

result and model prediction seems to occur at $l_w \approx \sigma$. This deviation is likely due to the inhomogeneous wall effect. In summary, it can seen that the analytically-based correction algorithms presented in this work are quite accurate in predicting the self-induced velocity encountered in actual EL simulations.

9 Relation to Other Correction Approaches

In this section, we briefly consider how the present approach relates to other approaches that have been proposed. In the case of other filter-based approaches, such as those using Wendland function [15], the primary difference is in the functional form of the filter and therefore the connection is clear. Depending on the nature of the filter function, the present approach can be extended either analytically or numerically to other filter functions.

Connection to correction methods that are not based on filtering or smoothening function is more subtle. Although the implementation details are more complex, the essence of the correction procedure advanced by Horwitz & Mani [21; 22] can be summarized in the present notation as

$$\mathbf{U} = \mathbf{u}_c + C\,(\Delta x)^2 \nabla^2 \mathbf{u}_c\,, \tag{47}$$

where $\mathbf{U}$ is the true undisturbed fluid velocity, while $\mathbf{u}_c$ is the disturbed fluid velocity obtained in an EL simulation. The constant C and its dependence on grid and particle size need to be calibrated as a pre-processing step. To establish the connection with the present approach, here, we have simplified the problem by ignoring volume fraction correction and also using the scalar correction. If we now use equation (7) to approximate the EL fluid velocity and its Laplacian, we obtain the relation

$$C = \frac{\Psi_{x\text{-}os}}{\Psi_{x\text{-}Lap}}\,\frac{\sigma^2}{\Delta x^2}\,. \tag{48}$$

A possible interpretation is as follows. In (47), the Laplacian of local fluid velocity acts as a sensor for the feedback force and the scaling factor C converts the feedback force into velocity correction, which when added to $\mathbf{u}_c$ recovers the undisturbed flow velocity. The expression (48) is only conceptual and not of practical value, since in the approach of Horwitz & Mani [21; 22] there is no filter width and the values of $\Psi_{x\text{-}os}$ and $\Psi_{x\text{-}Lap}$ are hard to define as well. It must however be noted that $\nabla^2\mathbf{u}_c$ in (47) must only be sensing the feedback force of a particle whose self-induced perturbation is being corrected. In situations where there are other particles in the immediate neighborhood, $\nabla^2\mathbf{u}_c$ at the location of a particle will not only be influenced by the feedback force of that particle, but also by the feedback force of the neighboring particles. Therefore care is required in separating out only the self-induced perturbation effect. Thus, the constant C calibrated for an isolated particle can be used in correction (47) only when the effect of neighbors is removed from $\nabla^2\mathbf{u}_c$.

The correction procedure of Esmaily and Horwitz [14] accounted for the time dependent nature of feedback force. If the quasi-steady limit, they expressed the force correction as (in the present notation)

$$\mathbf{F}'_{qs} = \left(1 - 0.75\frac{d_p}{\Delta x}\right)^{-1} \mathbf{F}'_{qs,EL}\,, \tag{49}$$

where the force on the left hand side is the true particle force, whereas the force on the right hand side is that evaluated in the EL simulation. As discussed earlier, this is precisely of the same form as the feedback correction given in (9). Equating the two, we obtain the relation

$$\frac{\Delta x}{\sigma} = \frac{0.75\sqrt{2\pi}}{\Phi\,\Psi_{x\text{-}os}}\,, \tag{50}$$

where we have replaced $\Psi_{x\text{-}ef}$ with $\Psi_{x\text{-}os}$ to account for the fact that their force calculation was without Faxén correction. Nevertheless, the above expression is only qualitative, since their numerical methodology was not based on a Gaussian filter. It should be noted that the correction given in (49) will work well even when a particle is surrounded by other neighbors, since the correction correctly attempts to undo only the effect of the self-induced feedback force and not those of the neighboring particles.

Finally, we consider the correction method of Pakseresht & Apte [31] using an auxiliary globally undisturbed flow solution. This method can be interpreted as numerically solving for the global perturbation flow $\mathbf{u}'_c$, along with the

velocity field $\mathbf{u}_c$ of the EL simulation. By combining the two as given in (5) the true undisturbed velocity field has been recovered. This approach has the advantage that the auxiliary solution $\mathbf{u}'_c$ is obtained by solving the complete non-linear equations in a time-dependent manner, unlike the steady Oseen approximation employed here. Furthermore, their correction procedure automatically accounts for the details of numerical methodology and thus is very good in the limit of isolated particles (i.e., very low volume fraction). As particle volume fraction increases, the difference between the EL velocity field and the globally undisturbed flow accounts for not only the self-induced perturbation flow, but also the perturbation effect of neighboring particles. However, only self-perturbation must be corrected for the correction procedure to be accurate. Thus, this approach will increasingly incur error with increasing particle volume fraction.

Of course, for each particle an auxiliary solution can be calculated only by ignoring the feedback force of that particle, while retaining the feedback of all other particles. In fact, this will be the true definition of undisturbed flow of the particle. Unfortunately, this approach is not computationally feasible, since as many auxiliary solutions as the number of particles in the system is required. In the present case, (12) and (51) along with the unsteady correction can be thought of as solving for the auxiliary problem, only with the feedback force of the particle removed, but in an approximate manner with the Oseen equation.

10 Conclusions

In this work we present a correction model of the self-induced perturbation velocity due to two-way coupling in Euler-Lagrange simulations. This model is based on Oseen solution of the incompressible perturbation flow resulting from a regularized feedback force. The present work improves upon the prior correction procedure of [5] in a few important ways. First, the correction procedure has been generalized to a vector form and thereby the directions of feedback force and relative velocity can be different. This allows the correction procedure to be used even in the presence of added-mass, history, and lift forces. Second, the effect of a nearby wall has been included in the correction procedure.

The correction procedure is developed around regularized Oseen solutions of streamwise and transverse forcing, whose analytical solutions are presented. In the simplest case of only quasi-steady force and without any wall effect, only the streamwise velocity of the streamwise regularized Oseenlet, and its Laplacian, Ψ_{os} and Ψ_{Lap} are required for the self-induced velocity correction. These functions are required only at the point of regularized forcing and thus they depend only on the Reynolds number Re_σ based on the Gaussian width. A vector form of the correction is developed to account for feedback forces other than quasi-steady contribution. In this case, three pairs of regularized Oseen functions are required in the implementation of the correction procedure. Once again, the Oseen functions are needed only at the point of regularized forcing and thus they depend on only Re_σ. With the inclusion of a nearby wall, the correction involves five pairs of regularized Oseen functions, each of which depends on Re_σ. However, the value of these functions is now required over the upper $x - y$ plane. In all these cases, step-by-step correction procedure involving these analytic functions is presented. Due to the implicit nature of the correction equation, an iterative approach is needed in the implementation of the correction. Numerical tests show that within three to four iterations convergence is achieved.

Numerical validation of the correction procedure was performed by comparing the self-induced velocity calculated in EL simulations against the corresponding predictions with the algorithms presented in this work. The vectorial correction Algorithm-1 was demonstrated to accurately predict both the streamwise and transverse components of self-induced velocity in the absence of a nearby wall. The prediction of the wall-induced correction Algorithm-2b was also compared against corresponding EL simulation results for varying particle-wall distances and force orientations relative to the flow direction. It is observed that prediction errors are small both for small and large particle-wall distance with the peak error occurring for $l_w \approx \sigma$ in the case of transverse force, which remains quite small compared to the force magnitude. Numerical validation has been performed only in the context of a particle being close to a single wall. There are less frequent instances of a particle being close to an edge or corner, where influences of multiple walls play a role. Although the correction algorithm in such situations has not been numerically evaluated, we expect the level of accuracy to remain quite good due to the additive nature of the wall corrections. But this along with the unsteady effects need to be further tested.

Another interesting challenging question is how to include the viscous effect of a nearby wall on the self-induced velocity. The viscous boundary layer involves more complicated particle-wall interaction and additional parameters

such as boundary layer thickness relative to the particle size and distance from the wall must be considered. The viscous effect of the wall is likely to be important when the wall is in the inner region of the perturbation flow. In the case of a particle smaller than the boundary layer, the general effect of a viscous wall is to hinder the relative velocity of a nearby particle due to the no-slip boundary condition. It can be anticipated that the self-induced velocity influenced by the viscous wall should be smaller than the inviscid wall condition. However, as the particle size increases relative to the boundary layer, the overall effect becomes difficult to anticipate and a more comprehensive self-induced velocity correction model is needed. It must also be pointed out that with the inclusion of the viscous effect, the correction model must consider the past history of the particle motion relative to the wall, thus, increasing the complexity of the modeling effort.

The correction Algorithms-1 and 2b implemented using the analytical regularized Oseen functions are observed to be accurate in predicting self-induced velocity correction computed in EL simulations employing finite difference, compact difference and other numerical discretization techniques, provided the numerical resolution is fine enough to resolve the spreading function. This desired level of accuracy is reached for $\Delta x \leq \sigma$ for spectral method and $\Delta x \leq \sigma/2$ for second-order finite difference method. If the discretization is not fine enough, the correction Algorithms-1 and 2b remain the same, however, they must use numerically obtained regularized Oseen functions. A step-by-step procedure for obtaining the required regularized Oseen functions using any EL code is presented in Algorithm-2a.

In addition to Gaussian spreading function, we have also considered hyper-Gaussian functions, which approximate the PIC approach. If the EL methodology used a feedback spreading function different from the Gaussian filter function, then the analytic regularized Oseen functions are qualitatively similar but quantitatively differed from the those of Gaussian spreading. For any other spreading function, the regularized Oseen functions can be either obtained analytically following the procedure used here (see Appendix A) or obtained numerically following the steps outlined in Algorithm-2a. Thus, the correction procedure presented here can be easily adapted to a wide variety of numerical simulations.

We finally note that this paper mostly focused on the quasi-steady problem. It has been shown in [5] that unsteady effects become important if there is rapid variation in the feedback force. In particular, [5] presented unsteady correction as an extension of the steady correction procedure and their unsteady correction model involves an additional convolution integral, whose history kernel has been presented as a function of delay time and Re_σ. In a strict sense, the derivation of the unsteady model must be repeated in the context of vector formulation and with the inclusion of wall effects in order to arrive at the proper unsteady model applicable for each numerical implementation. Here we prescribe an approximate unsteady correction procedure where we simply use the same unsteady kernel as was developed in [5] with the Φ function appropriately replaced.

A Solution of the Oseen Equation for Perturbation Velocity Field

We start with the following non-dimensional Oseens equation, where the feedback forcing $-\mathbf{F}'$ is centered at the origin and is arbitrarily oriented with all three non-zero components. In the analysis, we take the feedback force to be applied back on the fluid with a Gaussian spreading function G, whose width σ is chosen as the length scale of non-dimensionalization. The cross-stream velocity magnitude U_r is chosen as the velocity scale and the cross-stream flow is taken to be along the x-axis.

$$\begin{aligned} &\nabla \cdot (\phi_{1c}\mathbf{u}'_{1c}) = 0\,, \\ &\mathbf{e}_x \cdot \nabla (\phi_{1c}\mathbf{u}'_{1c}) = -\nabla p' + \frac{1}{\mathrm{Re}_\sigma}\nabla^2 (\phi_{1c}\mathbf{u}'_{1c}) - \mathbf{F}'G\,, \end{aligned} \tag{51}$$

Note that in this appendix all the quantities are non-dimensional. The above equations are solved in the spectral space and the procedure is the same as that presented in [5]. The resulting steady perturbation flow can be expressed by inverse Fourier transforming the solution in the spectral space as

$$[\phi_{1c}\mathbf{u}'_{1c}](\mathbf{r}) = \left[\frac{1}{(2\pi)^3}\iiint -\frac{\mathrm{Re}_\sigma}{k^2}\frac{1}{1+\dfrac{\iota\,\mathrm{Re}_\sigma\,k_x}{k^2}}\left(\mathbf{I}-\frac{\mathbf{k}\otimes\mathbf{k}}{k^2}\right)\exp\left(-\frac{k^2}{2}\right)\exp(\iota\mathbf{k}\cdot\mathbf{r})\,d\mathbf{k}\right]\mathbf{F}'\,, \tag{52}$$

where $\mathbf{k}$ is the non-dimensional wave-vector, whose magnitude is expressed as $k = |\mathbf{k}|$. In the above, $\mathbf{r}$ is the position vector where the perturbation velocity is being evaluated. We then write the term within the square parenthesis in the following form

$$\left[\phi_{1c}\mathbf{u}'_{1c}\right](\mathbf{r}) = -\frac{\mathrm{Re}_\sigma}{3\pi\sqrt{2\pi}}\begin{bmatrix} \Psi_{xx\text{-}os} & \Psi_{xy\text{-}os} & \Psi_{xz\text{-}os} \\ \Psi_{yx\text{-}os} & \Psi_{yy\text{-}os} & \Psi_{yz\text{-}os} \\ \Psi_{zx\text{-}os} & \Psi_{zy\text{-}os} & \Psi_{zz\text{-}os} \end{bmatrix}\mathbf{F}' \tag{53}$$

where the matrix of correction functions can be expressed as

$$\begin{bmatrix} \Psi_{xx\text{-}os} & \Psi_{xy\text{-}os} & \Psi_{xz\text{-}os} \\ \Psi_{yx\text{-}os} & \Psi_{yy\text{-}os} & \Psi_{yz\text{-}os} \\ \Psi_{zx\text{-}os} & \Psi_{zy\text{-}os} & \Psi_{zz\text{-}os} \end{bmatrix} = \frac{3}{2(2\pi)^{3/2}}\iiint \frac{1}{k^2}\frac{\left(\mathbf{I} - \dfrac{\mathbf{k}\otimes\mathbf{k}}{k^2}\right)}{1 + \dfrac{\iota\,\mathrm{Re}_\sigma\, k_x}{k^2}}\exp\left(-\frac{k^2}{2}\right)\exp\left(\iota\mathbf{k}\cdot\mathbf{r}\right)d\mathbf{k}\,. \tag{54}$$

We perform the above 3D integral in spherical coordinates by defining $\mathbf{k} = \{k\cos\theta, k\sin\theta\cos\varphi, k\sin\theta\sin\varphi\}$. Similarly we define the position vector in spherical coordinates as $\mathbf{r} = \{r\cos\alpha, k\sin\alpha\cos\beta, k\sin\alpha\sin\beta\}$. We desire the perturbation velocity only on the upper-half of the $x-y$ plane and therefore restrict $\beta = 0$ and vary $0 \le r \le \infty$ and $0 \le \alpha \le \pi$.

Integration over φ can be performed analytically, but integration over k and θ is carried out numerically. After integration over φ, only five components remain non-zero which can be obtain as

$$\begin{bmatrix} \Psi_{xx\text{-}os} & \Psi_{xy\text{-}os} & 0 \\ \Psi_{yx\text{-}os} & \Psi_{yy\text{-}os} & 0 \\ 0 & 0 & \Psi_{zz\text{-}os} \end{bmatrix} = \iint \frac{3\sin\theta\exp\left(-\dfrac{k^2}{2} + \iota kr\cos\theta\cos\alpha\right)}{2r\sqrt{2\pi}\left(k + \iota\,\mathrm{Re}_\sigma\cos\theta\right)}\begin{bmatrix} C_{xx} & C_{xy} & 0 \\ C_{xy} & C_{yy} & 0 \\ 0 & 0 & C_{zz} \end{bmatrix}dk\,d\theta\,. \tag{55}$$

where

$$C_{xx} = rk\sin\theta J_0\left(rk\sin\theta\sin\alpha\right)\,, \tag{56}$$

$$C_{yy} = rk\cos^2\theta J_0\left(rk\sin\theta\sin\alpha\right) + \sin\theta\csc\alpha J_1\left(rk\sin\theta\sin\alpha\right)\,, \tag{57}$$

$$C_{zz} = rkJ_0\left(rk\sin\theta\sin\alpha\right) - \sin\theta\csc\alpha J_1\left(rk\sin\theta\sin\alpha\right)\,, \tag{58}$$

$$C_{xy} = -\iota\frac{r}{2}k\sin\left(2\theta\right)J_1\left(rk\sin\theta\sin\alpha\right)\,, \tag{59}$$

$$C_{yx} = C_{xy}\,. \tag{60}$$

The Laplacian of the perturbation solution can be similarly expressed as the following integral in the wavenumber space

$$\nabla^2\left[\phi_{1c}\mathbf{u}'_{1c}\right](\mathbf{r}) = \left[\frac{1}{(2\pi)^3}\iiint \frac{\mathrm{Re}_\sigma}{1 + \dfrac{\iota\,\mathrm{Re}_\sigma\, k_x}{k^2}}\left(\mathbf{I} - \frac{\mathbf{k}\otimes\mathbf{k}}{k^2}\right)\exp\left(-\frac{k^2}{2}\right)\exp\left(\iota\mathbf{k}\cdot\mathbf{r}\right)d\mathbf{k}\right]\mathbf{F}'\,. \tag{61}$$

By following a similar approach the above integrals can be evaluated in spherical coordinates. Again, if we restrict the evaluation point to be on the $x-y$ plane, the φ integration can be analytically performed. We obtain the final form

$$\nabla^2\left[\phi_{1c}\mathbf{u}'_{1c}\right](\mathbf{r}) = -\frac{\mathrm{Re}_\sigma}{3\pi\sqrt{2\pi}}\begin{bmatrix} \Psi_{xx\text{-}Lap} & \Psi_{xy\text{-}Lap} & 0 \\ \Psi_{yx\text{-}Lap} & \Psi_{yy\text{-}Lap} & 0 \\ 0 & 0 & \Psi_{zz\text{-}Lap} \end{bmatrix}\mathbf{F}' \tag{62}$$

These Oseen and Laplace correction functions are plotted in Section 4.

B Convergence Rate of Iteration

In the convergence test, without loss of generality we set the non-dimensional *true* undisturbed relative velocity at the particle to be $\mathbf{U}_r = 1$ and the feedback force to be $-\mathbf{F}'_{qs} = (1, 0, 0)$. We considered varying scenarios for different

combinations of the following parameters: (i) Re_σ, (ii) d/σ, (iii) l/σ, (iv) α, and (v) the ratio $\mathbf{F}'_{ot}/|\mathbf{F}'_{qs}|$. These together cover all possible scenarios of iteration. For each parametric combination, the analytical self-induced velocity was obtained from which the self-perturbed velocity that would be computed in an EL simulation was evaluated. The test of iterative convergence then examines the following: given this self-perturbed EL velocity, how rapidly the iteration approaches the true undisturbed relative velocity at the particle. This requires the iteration procedure outlines in Algorithm-2b. At each iteration, the relative error between the true relative velocity and that estimated by the iterative algorithm is calculated and the result is shown in Figure 16. Figure 16a shows the rate of convergence for different combinations of Re_σ and d/σ. These are the two parameters given in the legend of Figure 16a. It can be observed that the rate of convergence first decreases and then increases with Re_σ and the slowest convergence is at around $\mathrm{Re}_\sigma = 1$. The rate of convergence increases as d_p/σ decreases. Figure 16b shows the rate of convergence for different combinations of l/σ and α, i.e., for different wall separations and wall orientations. The influence of l/σ and α is more complex and it is difficult to discern a definitive trend. Figure 16c shows the rate of convergence for different values of the three components of $\mathbf{F}'_{ot}/|\mathbf{F}'_{qs}|$, which are shown in the plot legend. Increasing the relative magnitude of the non-quasi-steady force slows the rate of convergence, especially if is oriented along the x-direction. While the other two components are about the same level in effect. Most importantly, in all cases two to three iterations are enough to recover the undisturbed velocity within about 1% of the true value.

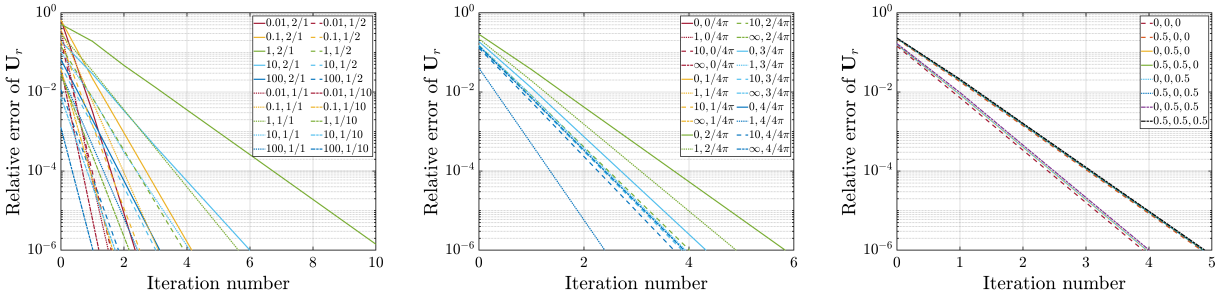

Figure 16: (a) Error plotted as a function of iteration number for different combinations of Re_σ and d/σ. (b) Error versus iteration number for different combinations of l/σ and α. (c) Error versus iteration number for different combinations of the ratio $\mathbf{F}'_{ot}/|\mathbf{F}'_{qs}|$.

Acknowledgments

This work was sponsored by the Office of Naval Research (ONR) as part of the Multidisciplinary University Research Initiatives (MURI) Program, under grant number N00014-16-1-2617. This work was also partially supported and benefited from the U.S. Department of Energy, National Nuclear Security Administration, Advanced Simulation and Computing Program, as a Cooperative Agreement to the University of Florida under the Predictive Science Academic Alliance Program, under Contract No. DE-NA0002378.

References

[1] Georges Akiki and S Balachandar. Immersed boundary method with non-uniform distribution of lagrangian markers for a non-uniform eulerian mesh. *Journal of Computational Physics*, 307:34–59, 2016.

[2] Hassan Aref and Sivaramakrishnan Balachandar. *A first course in computational fluid dynamics*. Cambridge University Press, 2017.

[3] S Balachandar. Lagrangian and eulerian drag models that are consistent between euler-lagrange and euler-euler (two-fluid) approaches for homogeneous systems. *Physical Review Fluids*, 5(8):084302, 2020.

[4] S Balachandar and John K Eaton. Turbulent dispersed multiphase flow. *Annual review of fluid mechanics*, 42:111–133, 2010.

[5] S Balachandar, Kai Liu, and Mandar Lakhote. Self-induced velocity correction for improved drag estimation in euler–lagrange point-particle simulations. *Journal of Computational Physics*, 376:160–185, 2019.

[6] S. Balachandar, Kai Liu, and Mandar Lakhote. Corrigendum to "Self-induced velocity correction for improved drag estimation in Euler–Lagrange point-particle simulations" [J. Comput. Phys. 376 (2019) 160–185]. *J. Comput. Phys.*, 401:108813, Jan 2020.

[7] GK Batchelor. *An introduction to fluid dynamics*. Cambridge university press, 2000.

[8] F Battista, P Gualtieri, J-P Mollicone, and CM Casciola. Application of the exact regularized point particle method (erpp) to particle laden turbulent shear flows in the two-way coupling regime. *International Journal of Multiphase Flow*, 101:113–124, 2018.

[9] Francesco Battista, J-P Mollicone, Paolo Gualtieri, Roberta Messina, and Carlo Massimo Casciola. Exact regularized point particle (erpp) method for particle-laden wall-bounded flows in the two-way coupling regime. *Journal of fluid mechanics*, 878:420, 2019.

[10] Jesse Capecelatro and Olivier Desjardins. An euler–lagrange strategy for simulating particle-laden flows. *Journal of Computational Physics*, 238:1–31, 2013.

[11] Éric Climent and Martin R Maxey. The force coupling method: a flexible approach for the simulation of particulate flows. 2009.

[12] Clayton Crowe, Martin Sommerfeld, Yutaka Tsuji, et al. *Multiphase flows with*. Ž, 1998.

[13] Clayton T Crowe, M Pt Sharma, and David E Stock. The particle-source-in cell (psi-cell) model for gas-droplet flows. 1977.

[14] Mahdi Esmaily and JAK Horwitz. A correction scheme for two-way coupled point-particle simulations on anisotropic grids. *Journal of Computational Physics*, 375:960–982, 2018.

[15] Fabien Evrard, Fabian Denner, and Berend van Wachem. Euler-lagrange modelling of dilute particle-laden flows with arbitrary particle-size to mesh-spacing ratio. *Journal of Computational Physics: X*, 8:100078, 2020.

[16] Toshiaki Fukada, Walter Fornari, Luca Brandt, Shintaro Takeuchi, and Takeo Kajishima. A numerical approach for particle-vortex interactions based on volume-averaged equations. *International Journal of Multiphase Flow*, 104:188–205, 2018.

[17] Toshiaki Fukada, Shintaro Takeuchi, and Takeo Kajishima. Interaction force and residual stress models for volume-averaged momentum equation for flow laden with particles of comparable diameter to computational grid width. *International Journal of Multiphase Flow*, 85:298–313, 2016.

[18] AJ Goldman, RG Cox, and H Brenner. Slow viscous motion of a sphere parallel to a plane wall—ii couette flow. *Chemical engineering science*, 22(4):653–660, 1967.

[19] Arthur Joseph Goldman, Raymond G Cox, and Howard Brenner. Slow viscous motion of a sphere parallel to a plane wall—i motion through a quiescent fluid. *Chemical engineering science*, 22(4):637–651, 1967.

[20] Paolo Gualtieri, F Picano, Gaetano Sardina, and Carlo Massimo Casciola. Exact regularized point particle method for multiphase flows in the two-way coupling regime. *Journal of Fluid Mechanics*, 773:520–561, 2015.

[21] JAK Horwitz and A Mani. Correction scheme for point-particle models applied to a nonlinear drag law in simulations of particle-fluid interaction. *International Journal of Multiphase Flow*, 101:74–84, 2018.

[22] JAK Horwitz and Ali Mani. Accurate calculation of stokes drag for point–particle tracking in two-way coupled flows. *Journal of Computational Physics*, 318:85–109, 2016.

[23] Peter J Ireland and Olivier Desjardins. Improving particle drag predictions in euler–lagrange simulations with two-way coupling. *Journal of Computational Physics*, 338:405–430, 2017.

[24] Gokul P Krishnan and David T Leighton Jr. Inertial lift on a moving sphere in contact with a plane wall in a shear flow. *Physics of Fluids*, 7(11):2538–2545, 1995.

[25] Hyungoo Lee and S Balachandar. Drag and lift forces on a spherical particle moving on a wall in a shear flow at finite re. *Journal of Fluid Mechanics*, 657:89, 2010.

[26] Kai Liu, Mandar Lakhote, and S Balachandar. Self-induced temperature correction for inter-phase heat transfer in euler-lagrange point-particle simulation. *Journal of Computational Physics*, 396:596–615, 2019.

[27] Sune Lomholt and Martin R Maxey. Force-coupling method for particulate two-phase flow: Stokes flow. *Journal of Computational Physics*, 184(2):381–405, 2003.

[28] Sune Lomholt and Martin R Maxey. Force-coupling method for particulate two-phase flow: Stokes flow. *Journal of Computational Physics*, 184(2):381–405, 2003.

[29] MR Maxey and BK Patel. Localized force representations for particles sedimenting in stokes flow. *International journal of multiphase flow*, 27(9):1603–1626, 2001.

[30] MR Maxey and BK Patel. Localized force representations for particles sedimenting in stokes flow. *International journal of multiphase flow*, 27(9):1603–1626, 2001.

[31] Pedram Pakseresht and Sourabh V Apte. A disturbance corrected point-particle approach for two-way coupled particle-laden flows on arbitrary shaped grids. *Journal of Computational Physics*, 439:110381, 2021.

[32] Pedram Pakseresht, Mahdi Esmaily, and Sourabh V Apte. A correction scheme for wall-bounded two-way coupled point-particle simulations. *Journal of Computational Physics*, 420:109711, 2020.

[33] Y Pan and S Banerjee. Numerical simulation of particle interactions with wall turbulence. *Physics of Fluids*, 8(10):2733–2755, 1996.

[34] Jean-François Poustis, Jean-Mathieu Senoner, Davide Zuzio, and Philippe Villedieu. Regularization of the lagrangian point force approximation for deterministic discrete particle simulations. *International Journal of Multiphase Flow*, 117:138–152, 2019.

[35] Alexandre M Roma, Charles S Peskin, and Marsha J Berger. An adaptive version of the immersed boundary method. *Journal of computational physics*, 153(2):509–534, 1999.

[36] PG Saffman. On the stability of laminar flow of a dusty gas. *Journal of fluid mechanics*, 13(1):120–128, 1962.

[37] Lanying Zeng, S Balachandar, and Paul Fischer. Wall-induced forces on a rigid sphere at finite reynolds number. *Journal of Fluid Mechanics*, 536:1–25, 2005.

[38] Lanying Zeng, Fady Najjar, S Balachandar, and Paul Fischer. Forces on a finite-sized particle located close to a wall in a linear shear flow. *Physics of fluids*, 21(3):033302, 2009.